Supplementary

A Novel Dialkylamino GFP Chromophore as an Environment-Polarity Sensor Reveals the Role of Twisted Intramolecular Charge Transfer

Cheng Chen [1], Sean A. Boulanger [1], Anatolii I. Sokolov [2,3], Mikhail S. Baranov [2,3] and Chong Fang [1,*,†]

[1] Department of Chemistry, Oregon State University, 153 Gilbert Hall, Corvallis, OR 97331, USA; chenc9@oregonstate.edu (C.C.); boulanse@oregonstate.edu (S.A.B.)
[2] Institute of Bioorganic Chemistry, Russian Academy of Sciences, Miklukho-Maklaya 16/10, 117997 Moscow, Russia; tonychem@yandex.ru (A.I.S.); baranovmikes@gmail.com (M.S.B.)
[3] Pirogov Russian National Research Medical University, Ostrovitianov 1, 117997 Moscow, Russia
* Correspondence: Chong.Fang@oregonstate.edu; Tel.: +1-541-737-6704
† Web: https://fanglab.oregonstate.edu/.

Table of Contents

1. Synthesis and characterization of intermediate compounds in Scheme 1

Methyl 3-hydroxy-4-nitrobenzoate (SAI286).

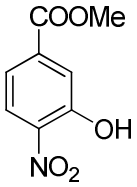

The titled compound was synthesized according to the previously published protocol, and the ^{1}H NMR spectrum matches the earlier report [1]. The ^{1}H NMR (700 MHz, DMSO-d_6) δ = 3.88 (s, 3H), 7.49 (dd, J = 8.5, 1.8 Hz, 1H), 7.68 (d, J = 1.8 Hz, 1H), 7.95 (d, J = 8.5 Hz, 1H), 11.44 ppm (s, 1H).

Methyl 4-amino-3-hydroxybenzoate (SAI288).

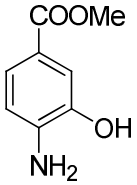

The titled compound was synthesized according to the previously published protocol. The ^{1}H NMR spectrum corresponded with the earlier report [1]. The ^{1}H NMR (300 MHz, DMSO-d_6) δ = 3.72 (s, 3H), 5.17 (broad singlet/brs, 2H), 6.59 (d, J = 8.6 Hz, 1H), 7.17 – 7.33 (m, 2H), 9.45 ppm (brs, 1H).

Methyl 4-(dimethylamino)-3-hydroxybenzoate (SAI145).

Methyl 4-amino-3-hydroxybenzoate (18.86 g, 112 mmol) and paraformaldehyde (7.05 g, 235.2 mmol) were dissolved in glacial acetic acid (100 mL). The mixture was then vigorously stirred at room temperature for 10 min. Sodium cyanoborohydride (15.44 g, 246.4 mmol) was added

portionwise to avoid foaming. The reaction flask was placed in an oil bath, carefully heated to 65 °C and stirred at that temperature for 3 hours. The reaction mixture was then poured in the aqueous solution of potassium hydroxide (78 g, 500 mL) to adjust the pH value to 7. The aqueous phase was extracted with ethyl acetate (2×250 mL). The solution was dried over Na_2SO_4, and the solvents were removed under reduced pressure. The crude product was purified with flash column chromatography (eluent – EtOAc/Hex, v/v = 1/2) to afford an off-white solid with a yield of 12.98 g (59%), m.p. = 103–105 °C.

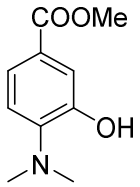

^{1}H NMR (700 MHz, DMSO-d_6) δ = 2.80 (s, 6H), 3.77 (s, 3H), 6.79 (d, J = 8.0 Hz, 1H), 7.28 – 7.44 (m, 2H), 9.54 ppm (s, 1H) (see Supplementary S7). ^{13}C NMR (75 MHz, DMSO-d_6) δ = 41.8, 51.6, 115.9, 116.6, 121.3, 121.5, 145.3, 148.4, 166.3 ppm (see Supplementary S8). HRMS (ESI) m/z $[M+H]^+$ calculated for $C_{10}H_{14}NO_3$: 196.0968, found: 196.0966.

Methyl 4-(dimethylamino)-3-((triisopropylsilyl)oxy)benzoate (SAI146).

Methyl 4-(dimethylamino)-3-hydroxybenzoate (12.06 g, 61.7 mmol) and imidazole (5.26 g, 77.13 mmol) were dissolved in acetonitrile (70 mL). Triisopropylsilyl chloride (15.86 ml, 74.04 mmol) was added dropwise, and the reaction mixture was subsequently left at room temperature overnight. The mixture was diluted with EtOAc (250 mL) and successively washed with water (2×100 ml) and brine (1×100 ml). The organic phase was dried over Na_2SO_4, until the solvents were evaporated. Flash column chromatography (eluent – EtOAc/Hex, v/v = 1/9) afforded the

desired product as colorless oil with a yield of 21.47 g (99%). The triisopropylsilyl (TIPS) ether group acts as a protecting group (the ether sidechain was noted as –OTIPS in Scheme 1, main text).

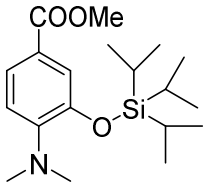

^{1}H NMR (700 MHz, DMSO-d_6) δ = 1.07 (d, J = 7.5 Hz, 18H), 1.26 (spt, J = 7.4 Hz, 3H), 2.81 (s, 6H), 3.78 (s, 3H), 6.92 (d, J = 8.3 Hz, 1H), 7.34 (d, J = 2.0 Hz, 1H), 7.50 ppm (dd, J = 8.4, 2.0 Hz, 1H) (see Supplementary S9). ^{13}C NMR (75 MHz, DMSO-d_6) δ = 12.3, 17.6, 42.0, 51.6, 117.2, 119.7, 121.5, 123.4, 146.7, 148.4, 165.9 ppm (see Supplementary S10). HRMS (ESI) m/z $[M+H]^+$ calculated for $C_{19}H_{34}NO_3Si$: 352.2302, found: 352.2296.

(4-(dimethylamino)-3-((triisopropylsilyl)oxy)phenyl)methanol (SAI150).

Lithium aluminum hydride (LAH; 5.28 g, 138.9 mmol) was dissolved in dry diethyl ether (150 mL) under an argon atmosphere; the flask was cooled to 0 °C. A solution of methyl 4-(dimethylamino)-3-((triisopropylsilyl)oxy)benzoate (21.23 g, 60.37 mmol) in Et_2O (40 mL) was added dropwise. The reaction mixture was stirred overnight. The excess of LAH was quenched with EtOAc (50 ml) and a solution of sodium hydroxide (5 M, 50 mL) was added. The reaction mixture was then diluted with Et_2O (400 mL) and washed successively with water (2×200 mL) and brine (1×200 ml). The organic phase was dried over Na_2SO_4, and the solvents were removed *in vacuo*. The residue was purified by flash column chromatography (gradient elution with EtOAc/Hex, v/v = 5/95 to 15/85) to afford the desired product as a yellowish oil with a yield of 16.02 g (82%).

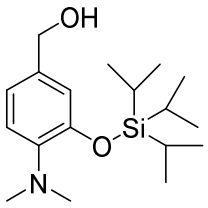

^{1}H NMR (700 MHz, DMSO-d_6), δ = 1.07 (d, J = 7.6 Hz, 18H), 1.26 (spt, J = 7.5 Hz, 3H), 2.66 (s, 6H), 4.36 (d, J = 5.7 Hz, 2H), 4.98 (t, J = 5.7 Hz, 1H), 6.76 – 6.80 (m, 2H), 6.81 – 6.85 ppm (m, 1H) (see Supplementary S11). ^{13}C NMR (75 MHz, DMSO-d_6), δ = 12.4, 17.8, 42.9, 62.5, 117.9, 117.9, 119.5, 136.3, 142.9, 148.0 ppm (see Supplementary S12). HRMS (ESI) m/z $[M+H]^+$ calculated for $C_{18}H_{34}NO_2Si$: 324.2353, found: 324.2349.

4-(dimethylamino)-3-((triisopropylsilyl)oxy)benzaldehyde (SAI157).

(4-(dimethylamino)-3-((triisopropylsilyl)oxy)phenyl)methanol (3.24 g, 10 mmol) was dissolved in dry DCM (40 mL). Pyridinium chlorochromate on alumina (33.33 g, 0.6 mmol/g, 20 mmol) was added and the reaction mixture was stirred at room temperature overnight. The mixture was then filtered through a pad of Celite. The solvents were removed under reduced pressure. The residue was purified by flash column chromatography (eluent – EtOAc/Hex, v/v = 3/97) to afford the desired product as a yellowish oil with a yield of 1.48 g (46%).

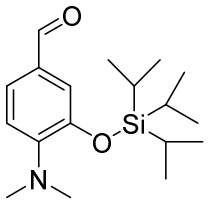

^{1}H NMR (700 MHz, DMSO-d_6) δ = 1.07 (d, J = 7.5 Hz, 18H), 1.29 (spt, J = 7.5 Hz, 3H), 2.87 (s, 6H), 6.99 (d, J = 8.2 Hz, 1H), 7.20 (d, J = 1.9 Hz, 1H), 7.46 (dd, J = 8.2, 1.9 Hz, 1H), 9.75 ppm (s, 1H) (see Supplementary S13). ^{13}C NMR (75 MHz, DMSO-d_6) δ = 12.4, 17.7, 42.0, 117.3,

117.4, 126.3, 129.1, 147.0, 149.9, 190.9 ppm (see Supplementary S14). HRMS (ESI) *m*/*z* [*M*+H]$^+$ calculated for $C_{18}H_{32}NO_2Si$: 322.2197, found: 322.2192.

(*Z*)-5-(4-(dimethylamino)-3-((triisopropylsilyl)oxy)benzylidene)-2,3-dimethyl-3,5-dihydro-4*H*-imidazol-4-one (SAI162).

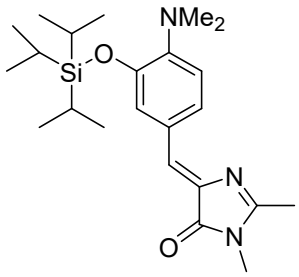

Eluent – EtOAc/Hex, v/v = 1/1. Yellow solid with a yield of 1.68 g (58%), m.p = 93–95 °C. ^{1}H NMR (700 MHz, DMSO-d_6) δ = 1.10 (d, *J* = 7.5 Hz, 18H), 1.37 – 1.44 (m, 3H), 2.31 (s, 3H), 2.82 (s, 6H), 3.08 (s, 3H), 6.83 – 6.85 (m, 2H), 7.34 (dd, *J* = 8.3, 1.9 Hz, 1H), 8.27 ppm (d, *J* = 1.9 Hz, 1H) (see Supplementary S15). ^{13}C NMR (176 MHz, DMSO-d_6) δ = 12.3, 15.2, 17.8, 26.1, 42.1, 117.1, 121.4, 125.2, 126.7, 127.3, 136.5, 145.9, 146.9, 161.8, 169.6 ppm (see Supplementary S16). HRMS (ESI) *m*/*z* [*M*+H]$^+$ calculated for $C_{23}H_{38}N_3O_2Si$: 416.2728, found: 416.2724.

1-methyl-1,2,3,4-tetrahydroquinoline (SAI287).

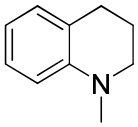

The titled compound was synthesized according to the previously published protocol. The ^{1}H NMR spectrum corresponded with the earlier reports [2]. The ^{1}H NMR (700 MHz, DMSO-d_6) δ = 1.83 – 1.91 (m, 2H), 2.67 (t, *J* = 6.5 Hz, 2H), 2.80 (s, 3H), 3.13 – 3.18 (m, 2H), 6.50 (td, *J* = 7.3, 1.2 Hz, 1H), 6.54 (dd, *J* = 8.2, 1.2 Hz, 1H), 6.84 – 6.88 (m, 1H), 6.93 – 6.99 ppm (m, 1H).

1-methyl-1,2,3,4-tetrahydroquinoline-6-carbaldehyde (SAI289).

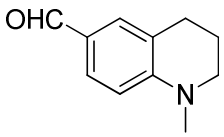

The titled compound was synthesized according to the previously published protocol. The ^{1}H NMR spectrum corresponded with the earlier reports [3]. The ^{1}H NMR (700 MHz, DMSO-d_6) δ = 1.87 (p, J = 6.1 Hz, 2H), 2.72 (t, J = 6.3 Hz, 2H), 2.97 (s, 3H), 3.33 – 3.38 (m, 2H), 6.63 (d, J = 8.6 Hz, 1H), 7.36 – 7.38 (m, 1H), 7.51 (dd, J = 8.5, 2.1 Hz, 1H), 9.59 ppm (s, 1H).

(*Z*)-2,3-dimethyl-5-((1-methyl-1,2,3,4-tetrahydroquinolin-6-yl)methylene)-3,5-dihydro-4*H*-imidazol-4-one (SAI295).

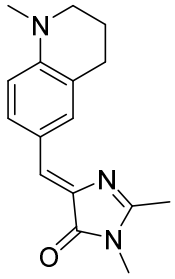

Red powder with a yield of 1.45 g (77%), m.p. = 189–191 °C. ^{1}H NMR (700 MHz, DMSO-d_6) δ = 1.88 (p, J = 6.2 Hz, 2H), 2.30 (s, 3H), 2.69 (t, J = 6.3 Hz, 2H), 2.93 (s, 3H), 3.07 (s, 3H), 3.31 (t, J = 5.7 Hz, 2H), 6.59 (d, J = 8.7 Hz, 1H), 6.79 (s, 1H), 7.78 (s, 1H), 7.86 ppm (d, J = 8.6 Hz, 1H) (see Supplementary S17). ^{13}C NMR (176 MHz, DMSO-d_6) δ = 15.1, 21.4, 26.1, 27.2, 38.3, 50.4, 110.1, 121.3, 121.7, 126.6, 132.4, 132.5, 134.2, 147.9, 159.8, 169.6 ppm (see Supplementary S18). HRMS (ESI) m/z $[M+H]^+$ calculated for $C_{16}H_{20}N_3O$: 270.1601, found: 270.1600.

Methyl 3-oxo-3,4-dihydro-2*H*-benzo[*b*][1,4]oxazine-7-carboxylate (SAI307).

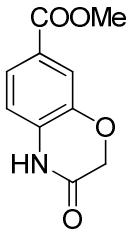

The titled compound was synthesized according to the previously published protocol. The ^{1}H NMR spectrum corresponded with the earlier report [4]. The ^{1}H NMR (700 MHz, DMSO-d_6) δ = 3.81 (s, 3H), 4.64 (s, 2H), 6.99 (d, J = 8.2 Hz, 1H), 7.43 (d, J = 1.8 Hz, 1H), 7.58 (dd, J = 8.2, 1.8 Hz, 1H), 11.04 ppm (s, 1H).

Methyl 3,4-dihydro-2*H*-benzo[*b*][1,4]oxazine-7-carboxylate (SAI312).

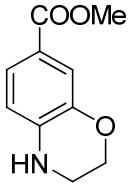

The titled compound was synthesized according to the previously published protocol. The ^{1}H NMR spectrum corresponded with the earlier reports in the literature [5]. The ^{1}H NMR (700 MHz, Chloroform-*d*) δ = 3.44 – 3.49 (m, 2H), 3.84 (s, 3H), 4.21 – 4.24 (m, 2H), 6.53 (d, J = 8.3 Hz, 1H), 7.45 (d, J = 1.9 Hz, 1H), 7.48 ppm (dd, J = 8.2, 1.9 Hz, 1H).

Methyl 4-methyl-3,4-dihydro-2*H*-benzo[*b*][1,4]oxazine-7-carboxylate (SAI315).

To a solution of methyl 3,4-dihydro-2*H*-benzo[*b*][1,4]oxazine-7-carboxylate (5.64 g, 29.17 mmol) in DMF (60 mL), potassium carbonate (4.43 g, 32.05 mmol) and methyl iodide (3.63 mL, 58.34 mmol) were added at room temperature. The reaction mixture was stirred for two hours before another portion of methyl iodide was added (1.81 mL, 29.17 mmol) and left to stir for reaction overnight. The reaction mixture was then diluted with ethyl acetate (200 mL), successively washed

with water (2×100 mL), saturated sodium thiosulfate solution (1×100 mL) and brine (2×100 mL). The organic phase was dried over Na_2SO_4. The solvents were then evaporated and the crude product was purified by flash column chromatography (eluent – EtOAc/Hex, v/v = 1/4) to afford a target compound as a white solid with a yield of 3.69 g (61%), m.p. = 56–58 °C.

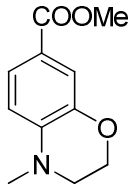

^{1}H NMR (700 MHz, DMSO-d_6) δ = 2.93 (s, 3H), 3.34 – 3.39 (m, 2H), 3.75 (s, 3H), 4.15 – 4.25 (m, 2H), 6.69 (d, J = 8.5 Hz, 1H), 7.18 (d, J = 2.0 Hz, 1H), 7.43 ppm (dd, J = 8.5, 2.0 Hz, 1H) (see Supplementary S19). ^{13}C NMR (176 MHz, DMSO-d_6) δ = 37.7, 47.9, 51.3, 63.8, 110.6, 115.6, 117.1, 123.7, 140.7, 142.5, 166.1 ppm (see Supplementary S20). HRMS (ESI) m/z $[M+H]^+$ calculated for $C_{11}H_{14}NO_3$: 208.0968, found: 208.0968.

(4-methyl-3,4-dihydro-2*H*-benzo[*b*][1,4]oxazin-7-yl)methanol (SAI319).

The reaction was conducted under an argon atmosphere. Methyl 4-methyl-3,4-dihydro-2*H*-benzo[*b*][1,4]oxazine-7-carboxylate (3.59 g, 17.34 mmol) was dissolved in dry toluene (40 ml) and the Schlenk flask was cooled in the an ice-cold water bath. A solution of DIBAL-H (1.5 M in toluene, 26 mL, 39 mmol) was added dropwise over the course of 10 minutes before the reaction was left to stir for an hour at 0 °C, and then warmed to room temperature. The progress was monitored with TLC (EtOAc/Hex, v/v = 1/1). As soon as the starting materials disappeared, water (10 mL) was carefully added to the mixture to quench the excess DIBAL-H, followed by the addition of a saturated solution of Rochelle salt (100 mL). This mixture was stirred for 30 minutes and passed through a pad of Celite. The pad was washed with ethyl acetate and the filtrate was

dried over Na_2SO_4. The solvents were removed *in vacuo*. The residue was purified by flash column chromatography (gradient elution with EtOAc/Hex, v/v = 6/94 to 50/50; a noticeable color change in this compound was observed while running the column) to afford the desired compound as a pale dark oil with a yield of 1.94 g (61%).

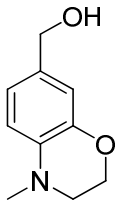

^{1}H NMR (700 MHz, DMSO-d_6) δ = 2.79 (s, 3H), 3.16 – 3.19 (m, 2H), 4.19 – 4.22 (m, 2H), 4.31 (d, J = 5.8 Hz, 2H), 4.86 (t, J = 5.7 Hz, 1H), 6.61 – 6.64 (m, 2H), 6.71 ppm (dd, J = 8.1, 1.9 Hz, 1H) (see Supplementary S21). ^{13}C NMR (176 MHz, DMSO-d_6) δ = 38.5, 48.6, 62.7, 64.4, 112.2, 114.1, 119.5, 132.2, 135.5, 143.7 ppm (see Supplementary S22). HRMS (ESI) m/z $[M+H]^+$ calculated for $C_{10}H_{14}NO_2$: 180.1019, found: 180.1016.

4-methyl-3,4-dihydro-2*H*-benzo[*b*][1,4]oxazine-7-carbaldehyde (SAI322).

(4-methyl-3,4-dihydro-2*H*-benzo[*b*][1,4]oxazin-7-yl)methanol (1.81 g, 10.11 mmol) was dissolved in dry DCM (50 mL). The reaction mixture was cooled in the ice-cold water bath. Dess-Martin periodinane (4.75 g, 12.63 mmol) was added portionwise over the period of 5 minutes. The reaction was left to stir for an hour at 0 °C and then warmed to room temperature. In 2 hours, the reaction mixture was diluted with 150 mL of ethyl acetate, washed with saturated potassium carbonate solution (2×70 mL), saturated potassium thiosulfate solution (2×70 mL) and brine (1×100 mL). The solution was dried over Na_2SO_4. The solvents were removed under reduced pressure and the leftover product was purified by flash column chromatography (eluent – EtOAc/Hex, v/v = 30/70; the substance was prone to decomposition and color change upon contact

with silica gel, therefore the column must be run quickly) to afford the desired compound as a dark oil with a yield of 0.934 g (52%).

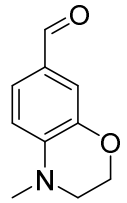

^{1}H NMR (700 MHz, DMSO-d_6) δ = 2.99 (s, 3H), 3.41 – 3.45 (m, 2H), 4.19 – 4.22 (m, 2H), 6.78 (d, J = 8.4 Hz, 1H), 7.11 (d, J = 1.9 Hz, 1H), 7.37 (dd, J = 8.3, 1.9 Hz, 1H), 9.62 ppm (s, 1H) (see Supplementary S23). ^{13}C NMR (176 MHz, DMSO-d_6) δ = 37.8, 47.9, 63.5, 110.5, 114.3, 125.6, 126.2, 142.1, 143.0, 189.9 ppm (see Supplementary S24). HRMS (ESI) m/z $[M+H]^+$ calculated for $C_{10}H_{12}NO_2$: 178.0863, found: 178.0859.

(*Z*)-2,3-dimethyl-5-((4-methyl-3,4-dihydro-2*H*-benzo[*b*][1,4]oxazin-7-yl)methylene)-3,5-dihydro-4*H*-imidazol-4-one (SAI326).

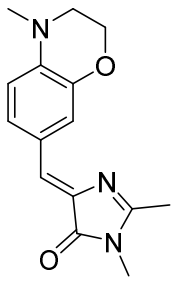

Orange solid with a yield of 665 mg (35%), m.p. = 209–211 °C. A mixture of E/Z isomers was isolated for this compound. The asterisk signs above some peaks (see the NMR spectrum in Supplementary S25 below) denote ones that belong to the isomeric admixture. ^{1}H NMR (700 MHz, DMSO-d_6) δ = 2.31 (s, 3H), 2.94 (s, 3H), 3.07 (s, 3H), 3.35 – 3.38 (m, 2H), 4.18 – 4.22 (m, 2H), 6.70 (d, J = 8.5 Hz, 1H), 6.80 (s, 1H), 7.51 (dd, J = 8.5, 2.0 Hz, 1H), 7.79 ppm (d, J = 2.0 Hz, 1H)

(see Supplementary S25). ^{13}C NMR (176 MHz, DMSO-d_6) δ = 15.2, 26.1, 37.7, 48.1, 63.8, 111.1, 118.0, 122.9, 126.0, 127.6, 135.2, 138.7, 143.0, 160.8, 169.6 ppm (see Supplementary S26). HRMS (ESI) *m*/*z* [*M*+H]$^+$ calculated for $C_{15}H_{18}N_3O_2$: 272.1394, found: 272.1394.

2. Supplementary Figures

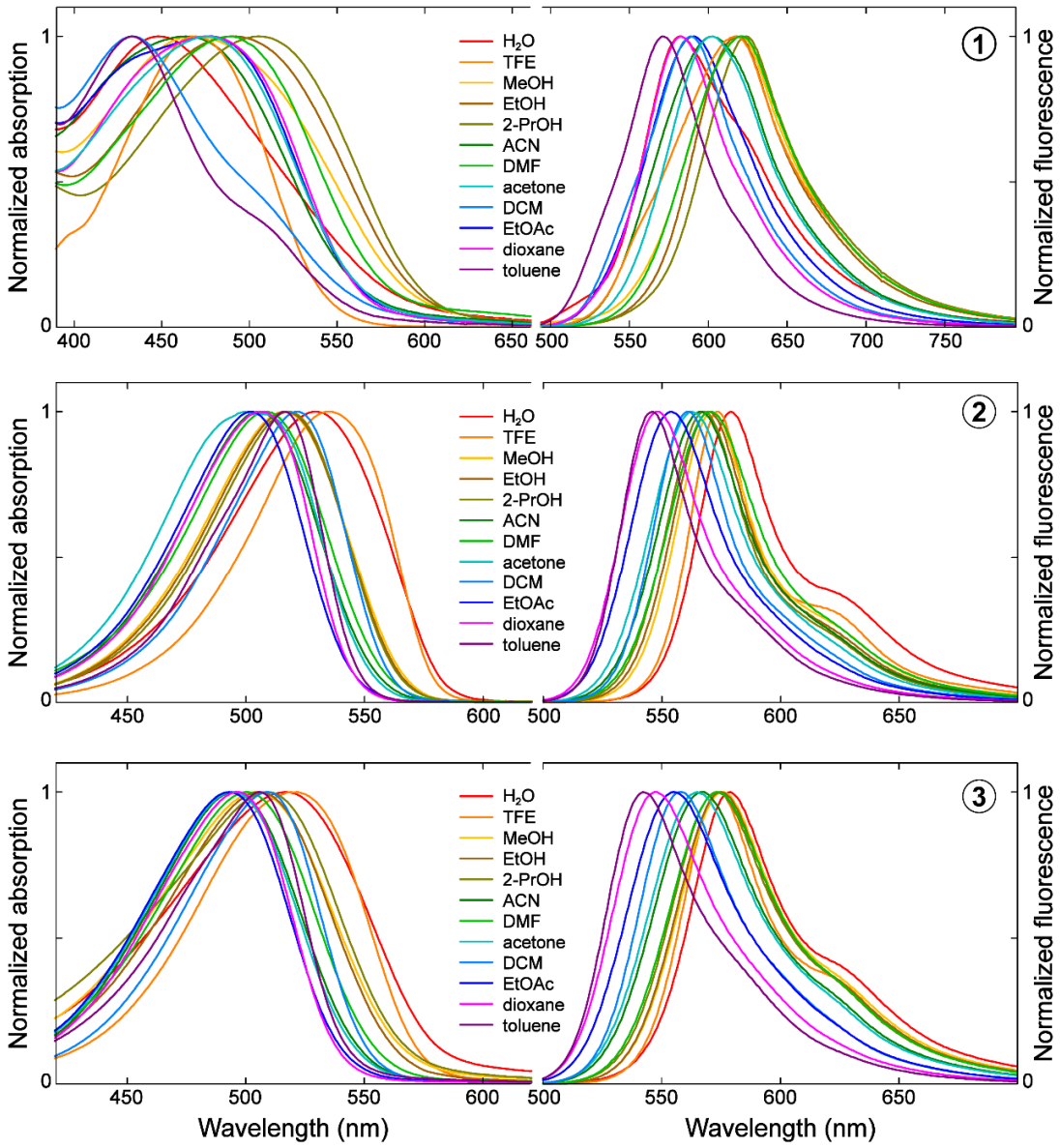

Figure S1. Steady-state absorption and emission spectra of compounds **1**, **2**, and **3** in various solvents at room temperature.

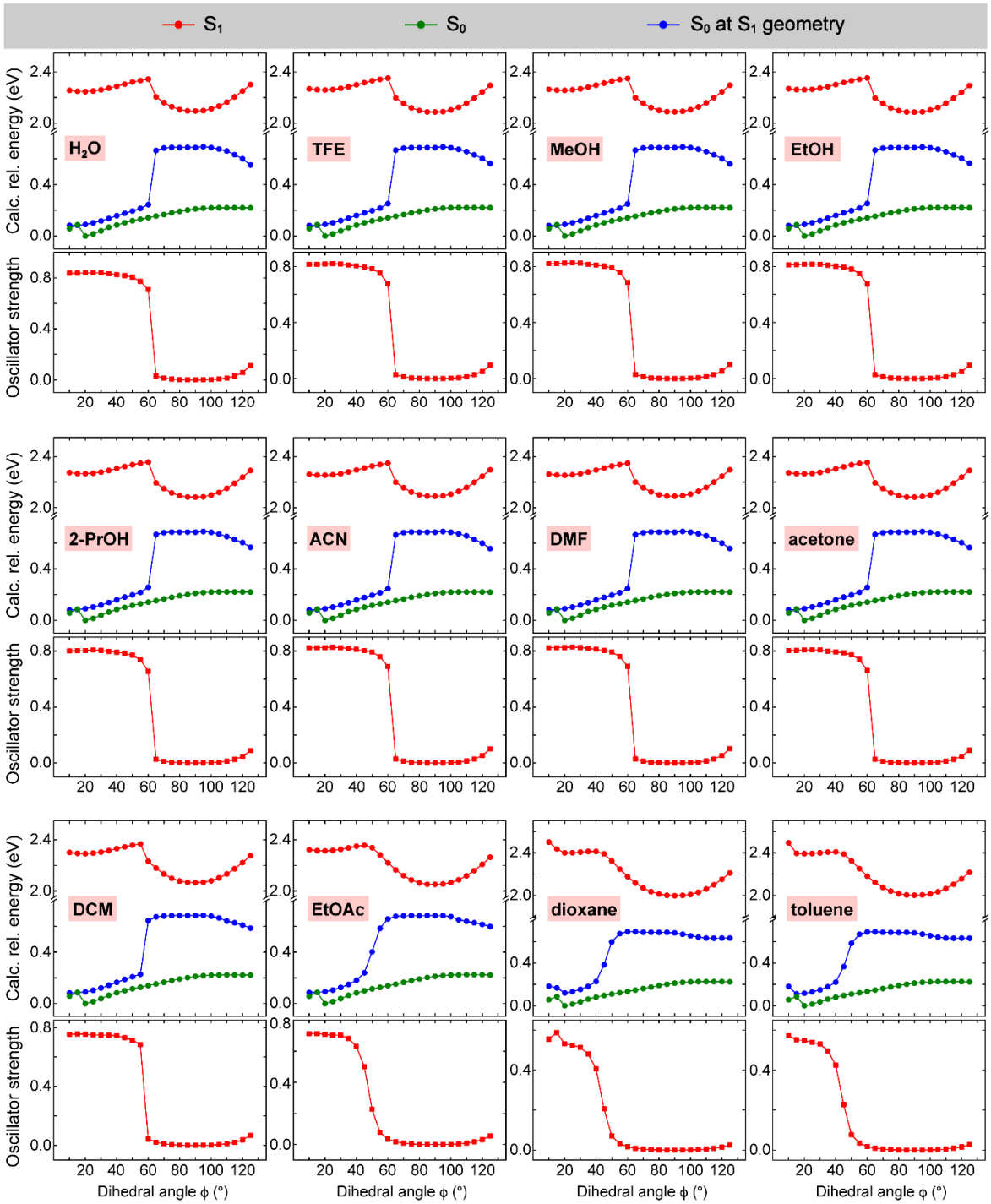

Figure S2. Calculated S_0 and S_1 potential energy surfaces and $S_1 \rightarrow S_0$ transition oscillator strength along the dimethylamine twisting coordinate ϕ for compound **1** in various solvents.

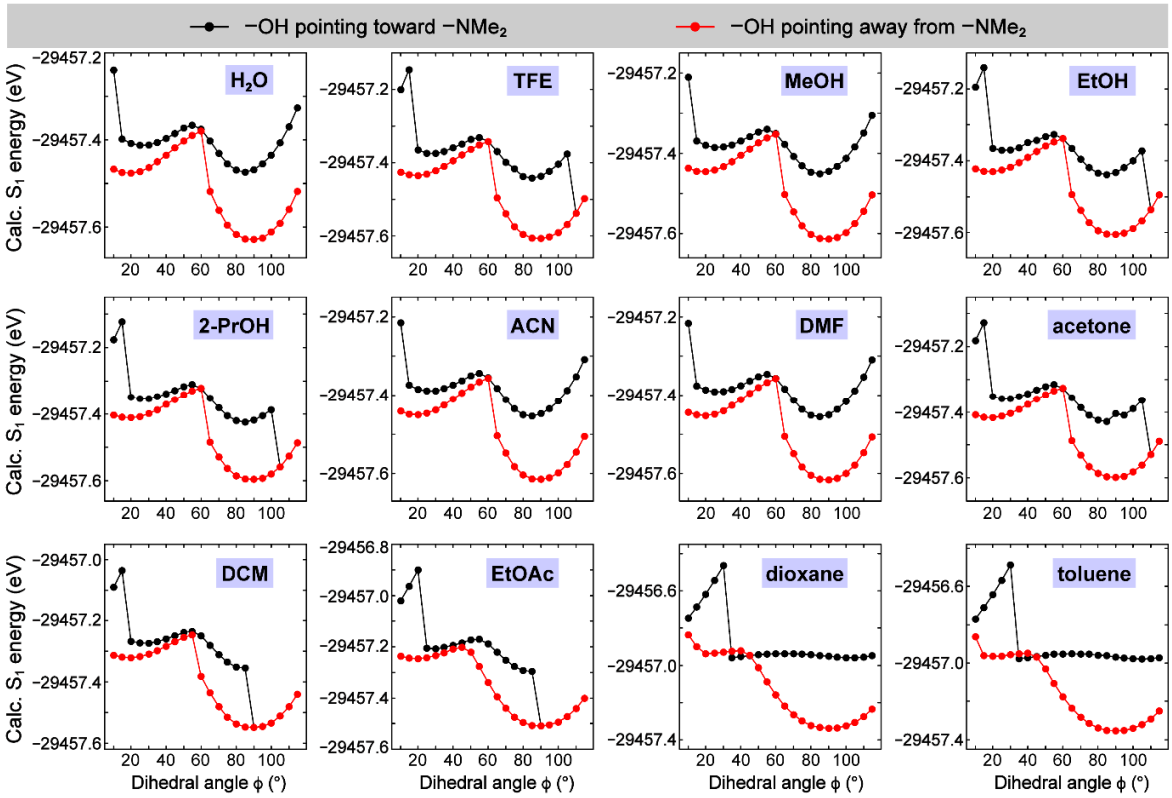

Figure S3. Calculated potential energy surfaces with different –OH group orientations for compound **1** in various solvents. The identical energies at large ϕ values for the two orientations in TFE, EtOH, 2-PrOH, acetone, DCM, and EtOAc are due to the flip of –OH group (on the chromophore P-ring) at convergence.

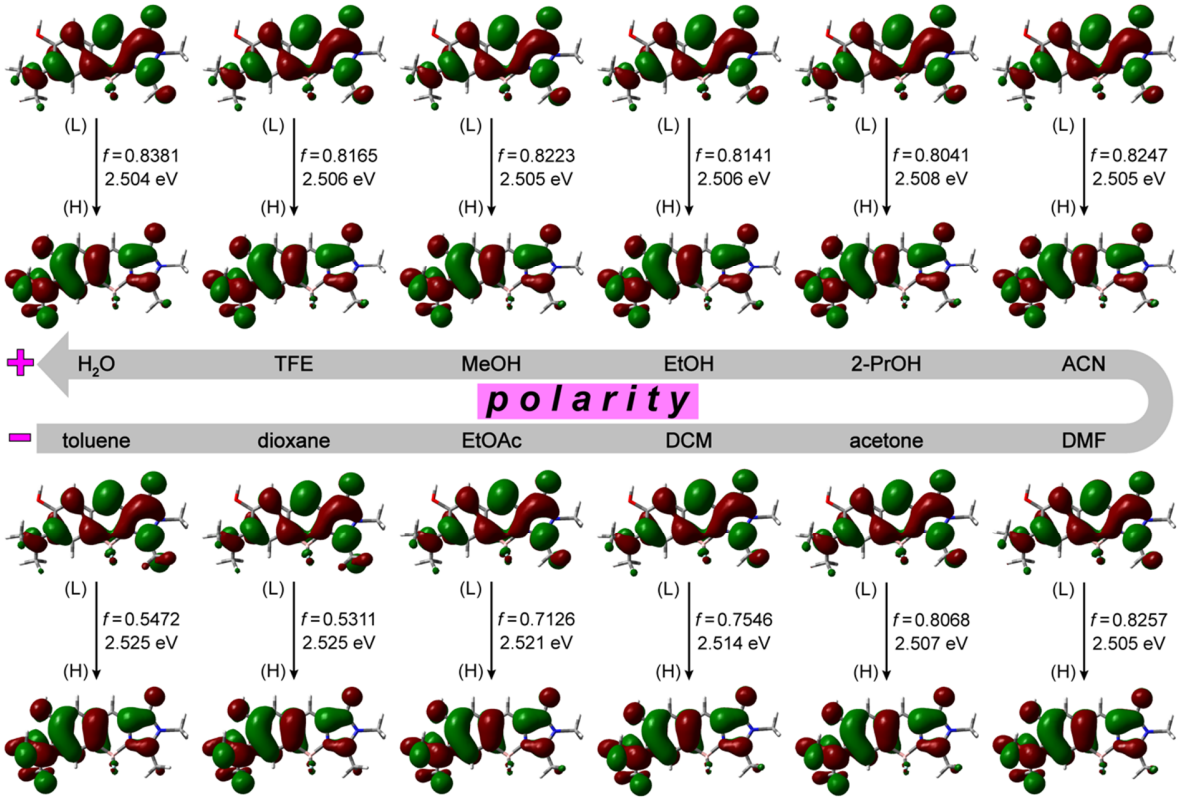

Figure S4. HOMO and LUMO electron density distributions for FS of compound **1**. The oscillator strength (f) and the HOMO–LUMO energy gap in eV unit are indicated by each vertical downward transition in various solvents with increasing polarity marked by the gray curved arrow (from the least polar toluene "–" to the most polar water "+", see Figure 1b in main text).

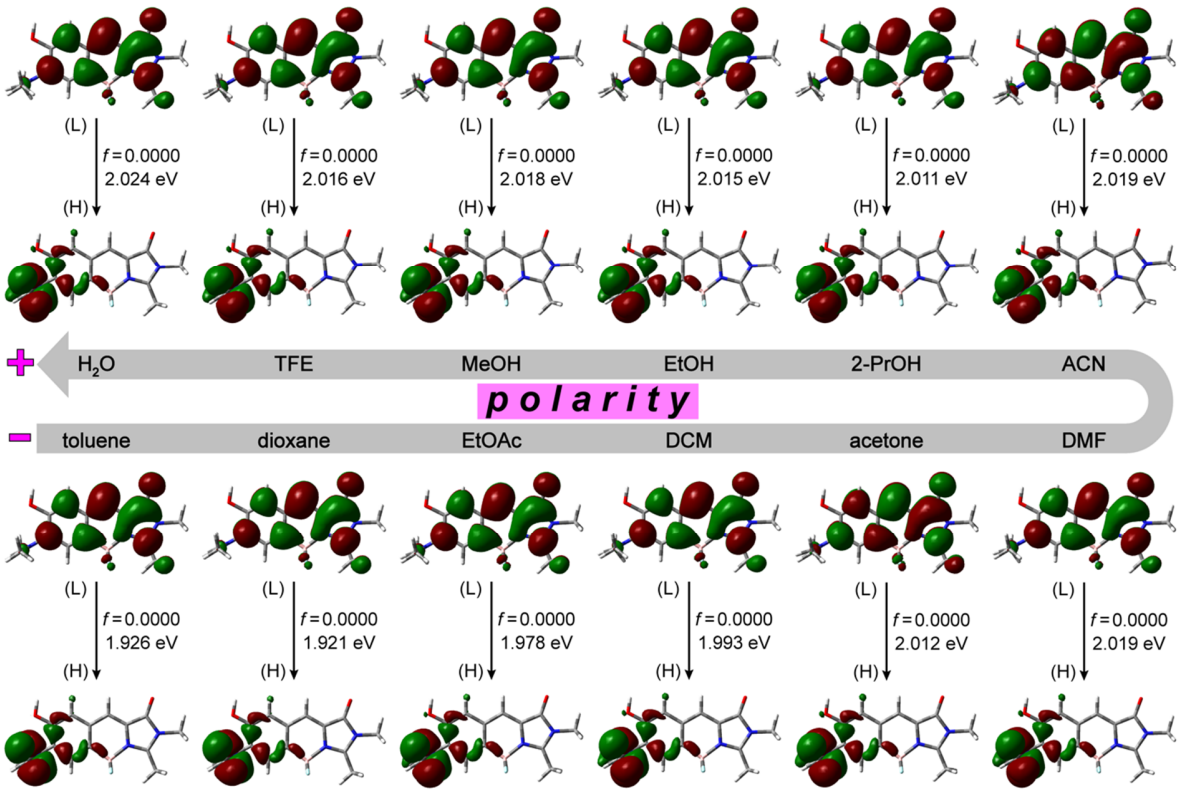

Figure S5. HOMO and LUMO electron density distributions for TICT state of compound **1**. The oscillator strength (f) and the HOMO–LUMO energy gap in eV unit are indicated by each vertical downward transition in various solvents with increasing polarity marked by the gray curved arrow (from the least polar toluene "–" to the most polar water "+", see Figure 1b in main text).

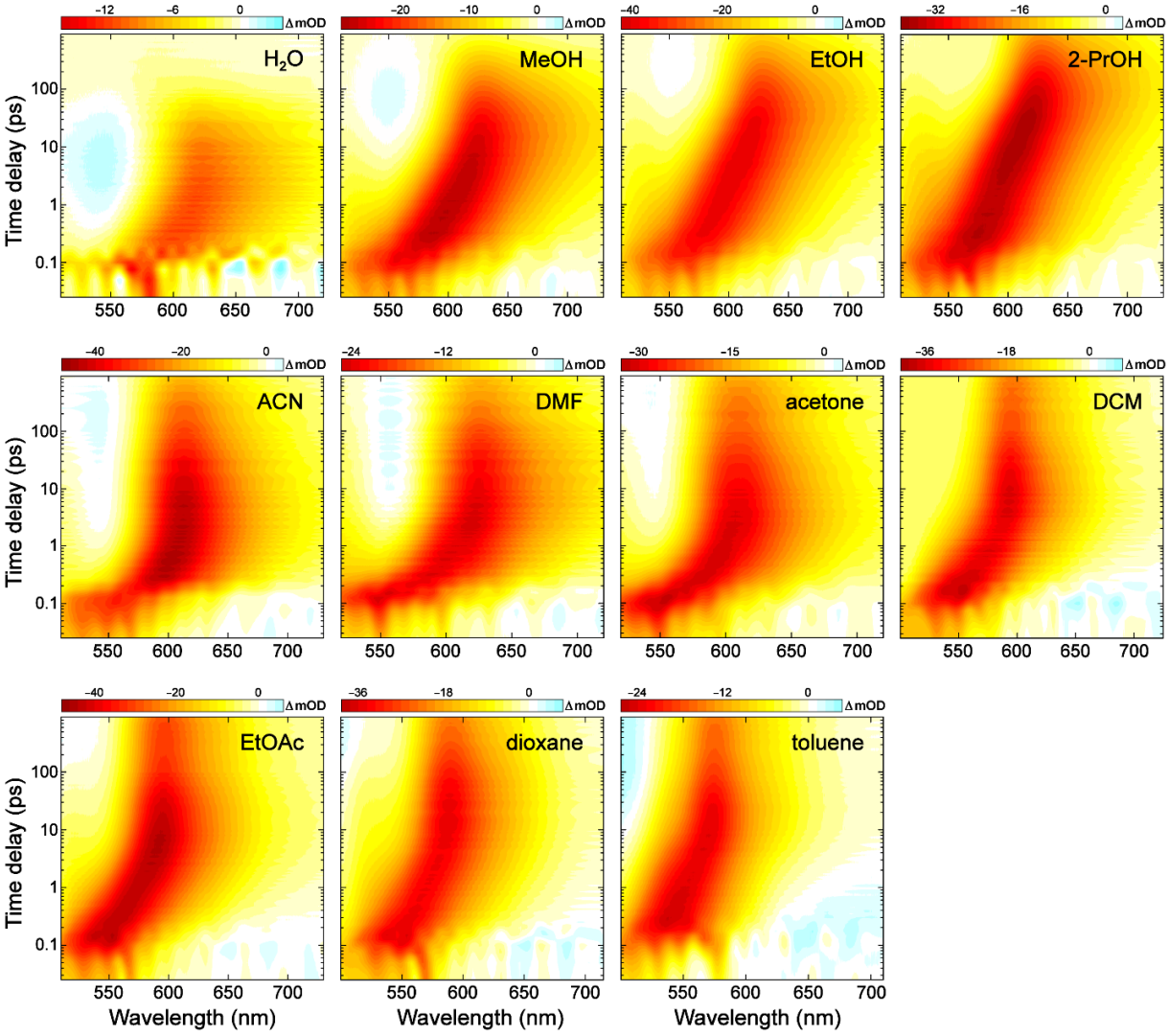

Figure S6. Contour plots of fs-TA spectra for compound **1** in 11 different solvents. The signal intensity color bars (in milli-optical density or mOD unit) are listed above each 2D contour plot. The corresponding TA spectra in TFE were excluded due to some apparent sample instability and a noticeable change of the steady-state UV/visible spectrum of compound **1** in TFE before and after the fs-TA measurements.

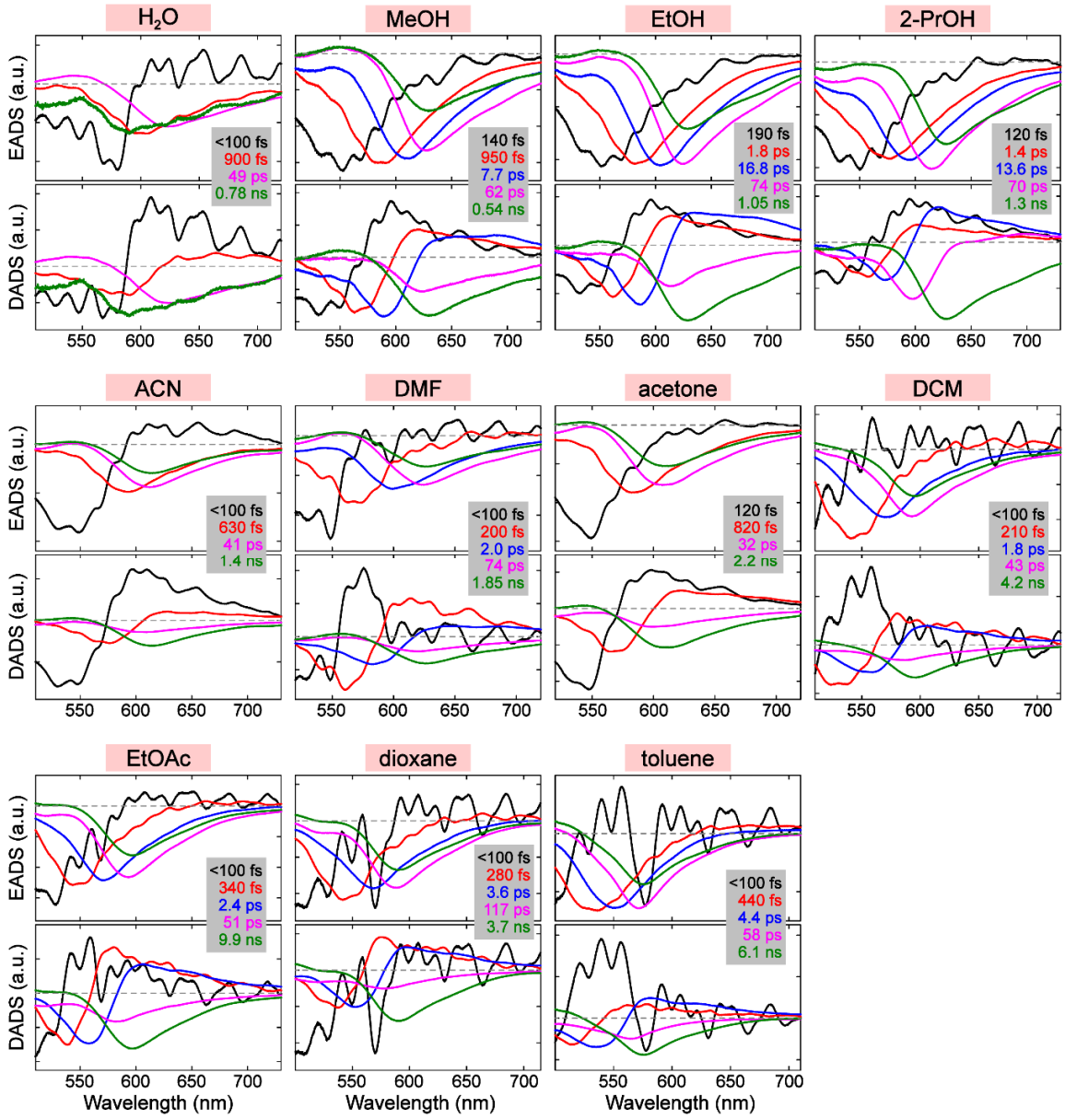

Figure S7. Global analysis of fs-TA spectra for compound **1** in 11 different solvents. The sequential kinetic scheme was adopted to retrieve the evolution-associated difference spectra (EADS, top panels) and lifetimes associated with pertinent transient species in the order of black→red(→blue)→magenta→green. The parallel kinetic scheme was adopted to retrieve the decay-associated difference spectra (DADS, bottom panels) for comparison [6,7] with associated lifetimes that are identical to EADS lifetimes (enclosed by the gray shaded rectangle in each inset).

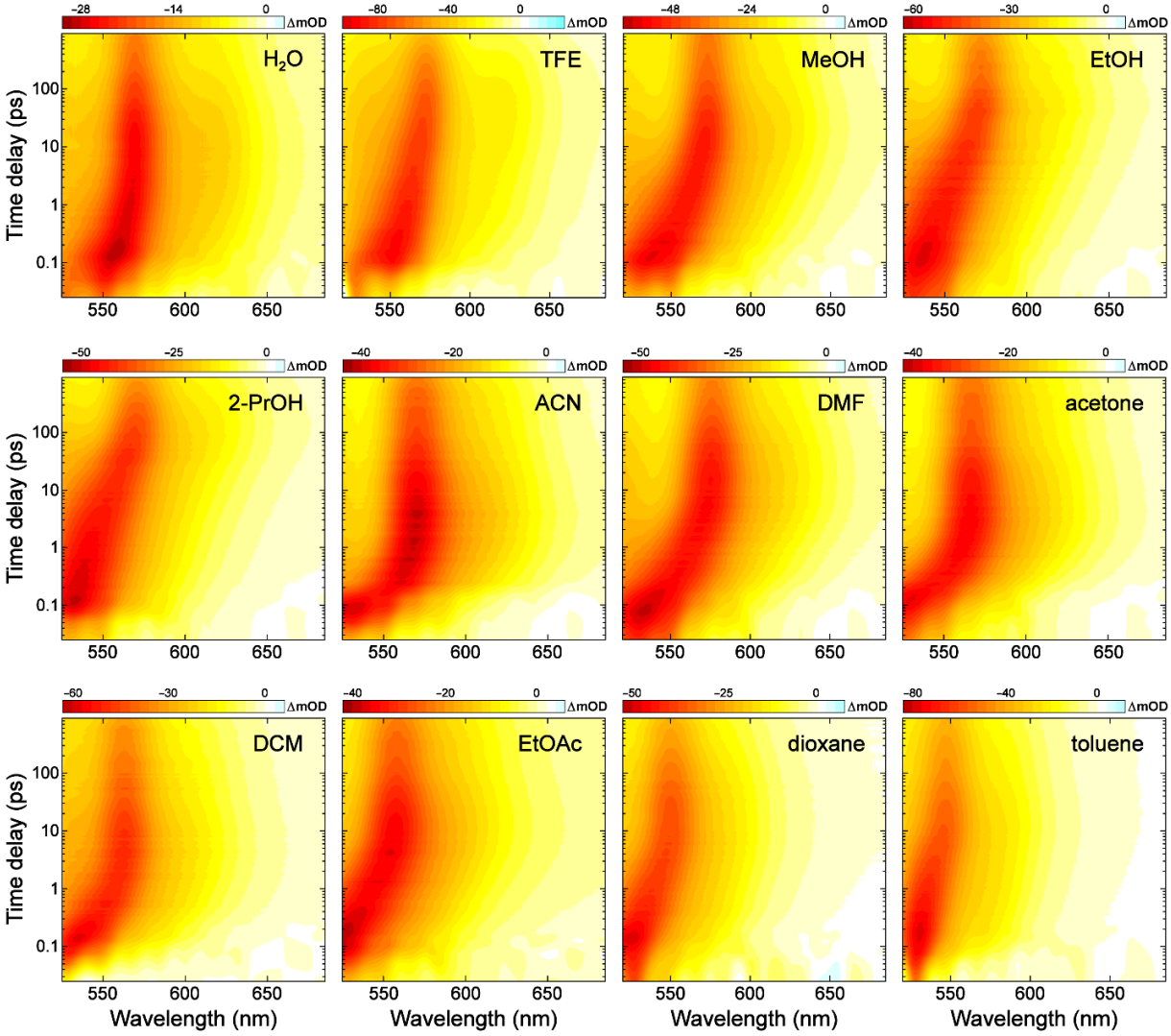

Figure S8. Contour plots of fs-TA spectra for compound **2** in 12 different solvents. The signal intensity color bars (in milli-optical density or mOD unit) are listed above each 2D contour plot.

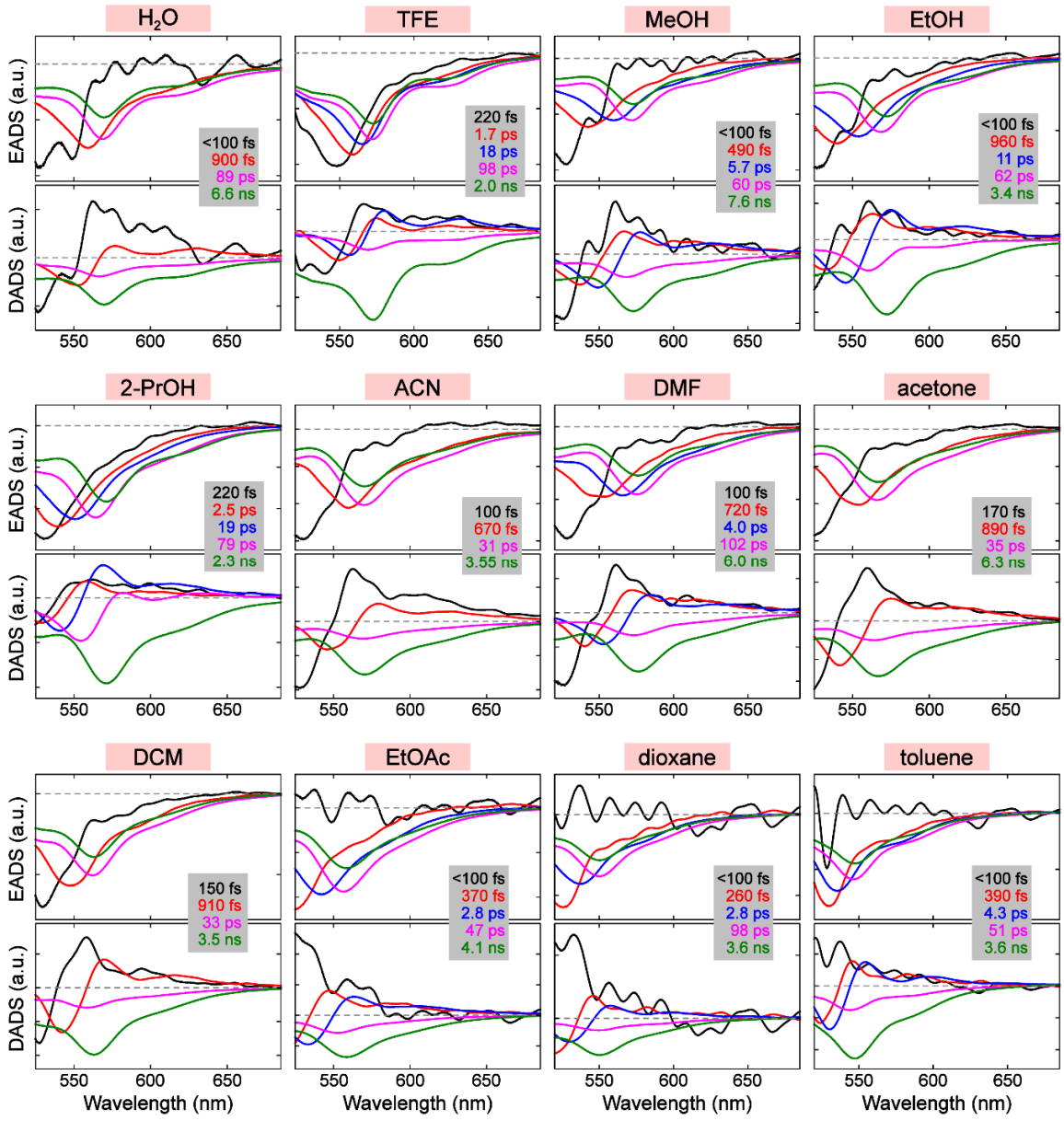

Figure S9. Global analysis of fs-TA spectra for compound **2** in 12 different solvents. The sequential kinetic scheme was adopted to retrieve the evolution-associated difference spectra (EADS, top panels) and lifetimes associated with pertinent transient species in the order of black→red(→blue)→magenta→green. The parallel kinetic scheme was adopted to retrieve the decay-associated difference spectra (DADS, bottom panels) for comparison and the associated lifetimes that are identical to EADS lifetimes (enclosed by the gray shaded rectangle in each inset).

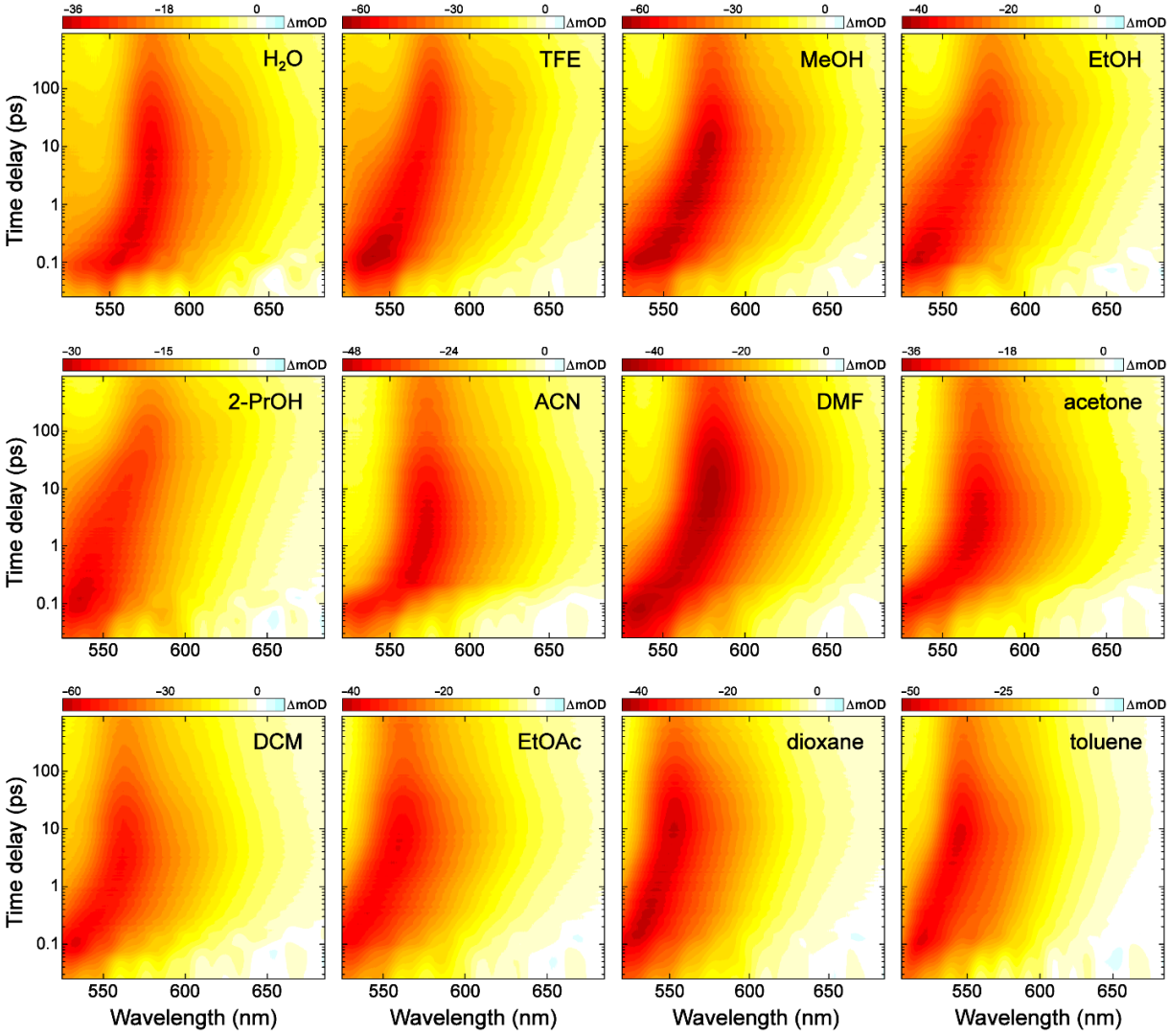

Figure S10. Contour plots of fs-TA spectra for compound **3** in 12 different solvents. The signal intensity color bars (in milli-optical density or mOD unit) are listed above each 2D contour plot.

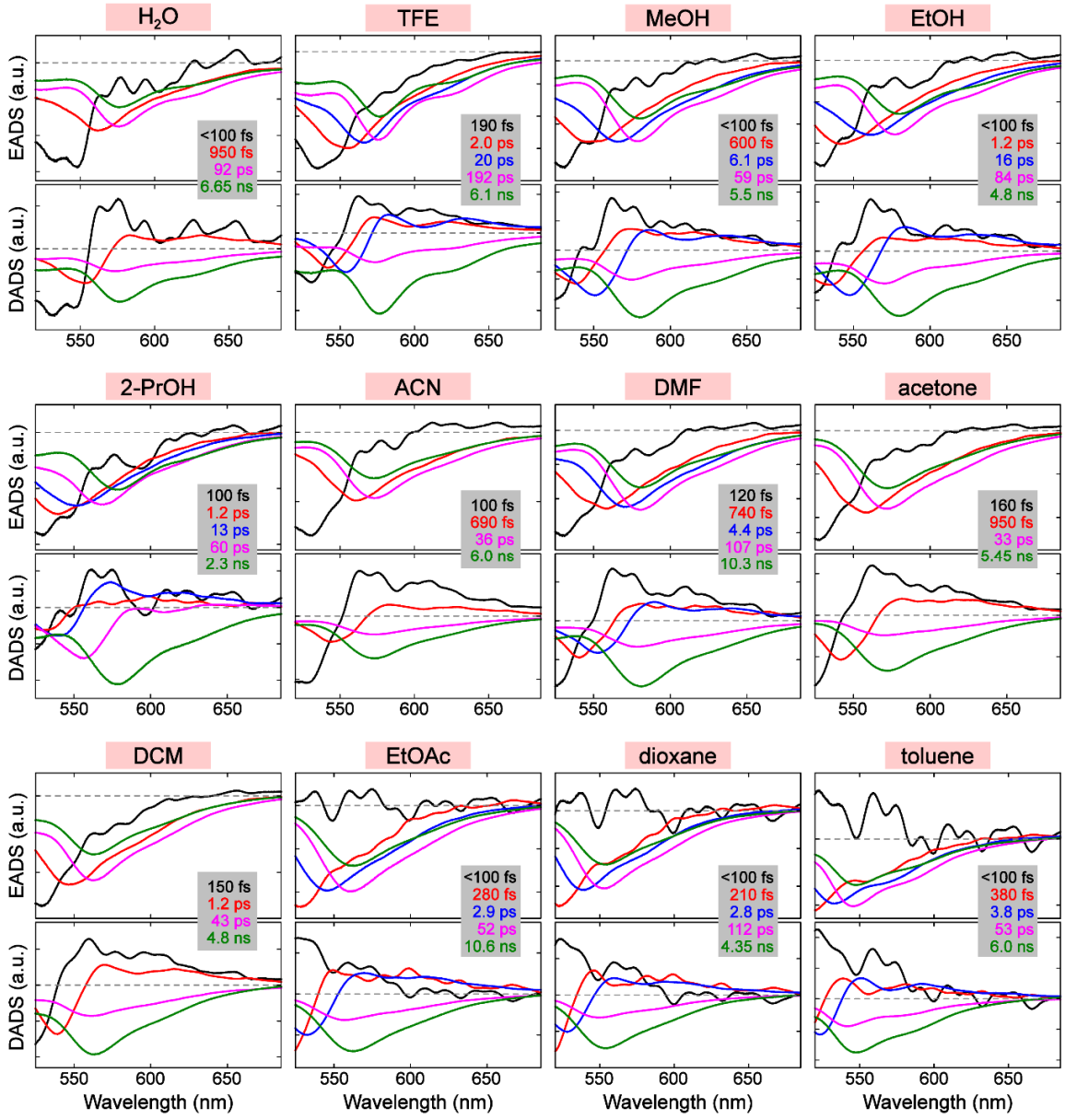

Figure S11. Global analysis of fs-TA spectra for compound **3** in 12 different solvents. The sequential kinetic scheme was adopted to retrieve the evolution-associated difference spectra (EADS, top panels) and lifetimes associated with pertinent transient species in the order of black→red(→blue)→magenta→green. The parallel kinetic scheme was adopted to retrieve the decay-associated difference spectra (DADS, bottom panels) for comparison and the associated lifetimes that are identical to EADS lifetimes (enclosed by the gray shaded rectangle in each inset).

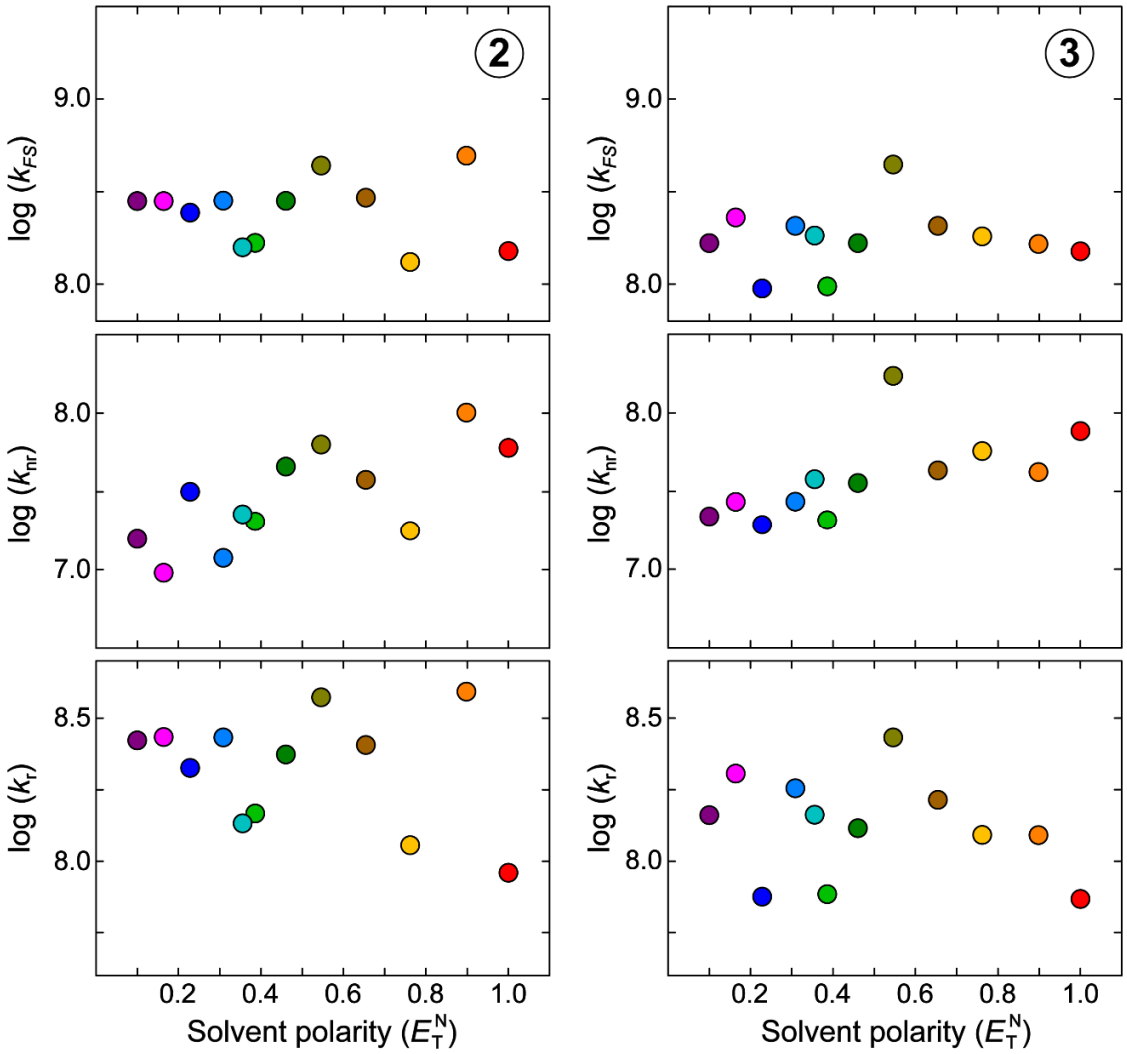

Figure S12. Relationships between decay rate constants and the solvent polarity parameter E_T^N for compounds **2** and **3**. The colors for solvents are defined the same way as Figure 1 (see main text) with the descriptions of all decay rate constants in relation to fluorescence quantum yield (FQY) summarized by Equations (3)–(5) (main text). The experimental fs-TA spectra with global analysis results are displayed in Figures S8 with S9 and Figures S10 with S11 for compounds **2** and **3**, respectively.

3. Supplementary Tables

Table S1. Kamlet-Taft analysis for absorption and emission of compounds **1**, **2**, and **3**

Compound	Coeff.[a]	absorption[b]			emission[b]		
		value	*p*-value	R^2	value	*p*-value	R^2
1	a	Not available[c]			−0.40	0.1478	0.49
	b				−0.96	0.0639	
	p				0.21	0.7833	
	v_0				17.1	9.5×10^{-10}	
2	a	−0.60	0.0006	0.84	−0.34	0.0029	0.87
	b	0.44	0.0584		−0.44	0.0167	
	p	−0.19	0.5716		−0.90	0.0059	
	v_0	19.7	4.8×10^{-13}		18.7	6.6×10^{-14}	
3	a	−0.51	0.0023	0.78	−0.40	0.0048	0.85
	b	0.32	0.1587		−0.73	0.0048	
	p	−0.24	0.4997		−0.89	0.0212	
	v_0	20.1	5.8×10^{-13}		18.8	4.5×10^{-13}	

[a] The spectral shift ν and fit intercept ν_0 have the 10^3 cm^{-1} unit (see Equation (2) in main text).

[b] The statistically significant coefficients (ca. $p \leq 0.05$) are highlighted by light orange shades.

[c] Cannot be reliably obtained due to the complex absorption profile of compound **1** (see Figure S1 top left panel).

Extended discussion for Table S1:

The electronic absorption peak of compounds **2** and **3** shows a prominent dependence on the solvent H-bonding capability (α and/or β), while the negative coefficient of α (a<0) and positive coefficient of β (b>0 for compound **2** only, with statistical significance) indicate the strengthening and weakening of the H-bond accepting and donating capability of the chromophore,

respectively, from the electronic ground (S_0) to excited state (S_1) at the thermally equilibrated S_0 geometry [8,9].

The electronic emission (fluorescence peak) of compounds **2** and **3** exhibits different dependence on solvent polarity from compound **1**. The common dependence on β (solvent basicity) with a negative coefficient (b<0) indicates the strengthening of the H-bond donating capability (solute acidity) of the chromophore from S_0 to S_1 at the relaxed S_1 geometry, which is particularly prominent (i.e., largest magnitude of 0.96) for compound **1**. Compounds **2** and **3** also show a similar dependence on α and π^* and the negative coefficients for both parameters (a<0, p<0) suggest that the H-bond accepting capability and dipole moment of the chromophore increase from S_0 to S_1 at the relaxed S_1 geometry, whereas such a change in properties becomes insignificant for compound **1** with pronounced fluorogenicity (see main text).

Notably, the calculated electronic density maps of HOMO and LUMO at the FS state of compound **1** (for vertical electronic emission, see Figure S4) show a clear decrease in the electron density at the –OH group from S_0 to S_1, which is consistent with the aforementioned increase in the H-bond donating capability of compound **1** that seems to dominate the solvatochromic behavior of its emission peak (Table S1) and contribute to its fluorescence properties in various solvents.

Table S2. Photophysical properties of compounds **1**, **2**, and **3** in various solvents

Compound	solvent	solvent properties			λ_{abs} [a] (nm)	λ_{em} (nm)	Φ (%)
		α	β	π^*			
1 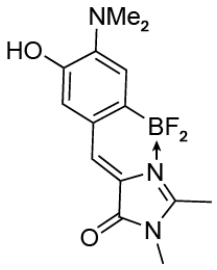	H_2O	1.17	0.4	1.09	448	582	2.0
	TFE	1.51	0	0.73	469	617	3.6
	MeOH	0.93	0.62	0.60	468	620	6.0
	EtOH	0.83	0.77	0.54	490	618	12.5
	2-PrOH	0.76	0.84	0.48	505	624	16.4
	ACN	0.19	0.31	0.66	464	603	15.9
	DMF	0	0.69	0.88	489	621	14.8
	acetone	0.08	0.48	0.62	476	602	29.6
	DCM	0.3	0	0.73	433	589	62.6
	EtOAc	0	0.45	0.55	477	590	46.3
	dioxane	0	0.37	0.49	476	583	59.2
	toluene	0	0.11	0.49	433	571	69.3
2 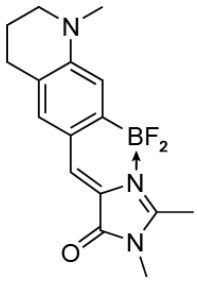	H_2O	1.17	0.4	1.09	529	579	60.2
	TFE	1.51	0	0.73	535	573	79.5
	MeOH	0.93	0.62	0.60	516	571	86.5
	EtOH	0.83	0.77	0.54	517	570	87.1
	2-PrOH	0.76	0.84	0.48	518	568	85.5
	ACN	0.19	0.31	0.66	505	566	83.8
	DMF	0	0.69	0.88	508	570	87.8
	acetone	0.08	0.48	0.62	503	563	85.6
	DCM	0.3	0	0.73	521.5	561	95.8
	EtOAc	0	0.45	0.55	502	554	87.0
	dioxane	0	0.37	0.49	506	548	96.6
	toluene	0	0.11	0.49	516	546	94.4
3 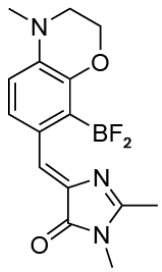	H_2O	1.17	0.4	1.09	517	579	49.0
	TFE	1.51	0	0.73	521	574	74.6
	MeOH	0.93	0.62	0.60	504	575.5	68.3
	EtOH	0.83	0.77	0.54	505.5	575	79.2
	2-PrOH	0.76	0.84	0.48	509	573	61.2
	ACN	0.19	0.31	0.66	495	567	78.4
	DMF	0	0.69	0.88	500.5	574	78.7
	acetone	0.08	0.48	0.62	494.5	565	79.3
	DCM	0.3	0	0.73	509	558	86.8
	EtOAc	0	0.45	0.55	493	555	79.5
	dioxane	0	0.37	0.49	497	547	88.2
	toluene	0	0.11	0.49	506	542	86.8

[a] The absorption peak wavelengths of compound **1** may not be accurate due to the complex profile (Figure S1 top left panel). In water (pH=7.4 PBS buffer), compound **1** remains protonated. The FQY (last column) histogram plots for compounds **1** and **2**, **3** are in Figure 1c and 1d, respectively.

Table S3. Calculated optical and structural properties for compound **1** in various solvents

	Solvent	HOMO (eV)	LUMO (eV)	LUMO–HOMO gap (eV) [a]	λ_{em} (nm) [b]	oscillator strength	dihedral angles ϕ, ϕ' (°) [c]	dipole moment (Debye)
FS	H_2O	–5.3449	–2.8406	2.5043	574.2	0.8381	–18.8, 142.1	0.546
	TFE	–5.3419	–2.8360	2.5059	571.3	0.8165	–18.9, 141.2	0.591
	MeOH	–5.3424	–2.8371	2.5054	572.1	0.8223	–18.9, 141.5	0.574
	EtOH	–5.3419	–2.8354	2.5064	570.9	0.8141	–18.9, 141.1	0.599
	2-PrOH	–5.3413	–2.8338	2.5075	569.5	0.8041	–18.9, 140.7	0.635
	ACN	–5.3424	–2.8376	2.5048	572.4	0.8247	–18.9, 141.6	0.566
	DMF	–5.3427	–2.8379	2.5048	572.5	0.8257	–18.9, 141.6	0.565
	acetone	–5.3413	–2.8341	2.5073	569.9	0.8068	–18.9, 140.8	0.626
	DCM	–5.3413	–2.8270	2.5143	563.0	0.7546	–19.0, 138.4	0.857
	EtOAc	–5.3438	–2.8232	2.5206	557.7	0.7126	–19.2, 136.4	1.068
	dioxane	–5.3408	–2.8153	2.5255	544.0	0.5311	–20.5, 129.8	1.719
	toluene	–5.3416	–2.8161	2.5255	545.1	0.5472	–20.4, 130.3	1.673
TICT	H_2O	–5.2415	–3.2175	2.0240	881.0	0	90.0, –87.7	4.865
	TFE	–5.2300	–3.2142	2.0158	885.8	0	89.9, –87.9	4.813
	MeOH	–5.2330	–3.2150	2.0180	884.4	0	89.8, –87.9	4.830
	EtOH	–5.2284	–3.2137	2.0147	886.3	0	89.8, –87.9	4.810
	2-PrOH	–5.2227	–3.2118	2.0109	888.5	0	89.8, –87.9	4.790
	ACN	–5.2341	–3.2150	2.0191	884.0	0	89.9, –87.8	4.836
	DMF	–5.2349	–3.2156	2.0193	883.6	0	89.9, –87.9	4.837
	acetone	–5.2240	–3.2120	2.0120	887.8	0	89.8, –87.9	4.798
	DCM	–5.1966	–3.2036	1.9930	898.7	0	89.8, –88.2	4.696
	EtOAc	–5.1753	–3.1971	1.9782	907.2	0	89.8, –87.4	4.625
	dioxane	–5.0962	–3.1750	1.9212	940.9	0	90.8, –90.3	4.365
	toluene	–5.1030	–3.1769	1.9261	937.8	0	90.7, –90.1	4.389

[a] The calculated electron density maps of HOMO (H) and LUMO (L) for the FS and TICT states are displayed in Figures S4 and S5, respectively, as a function of solvent polarity.

[b] The calculated emission peak wavelength was retrieved from the output emission spectrum from a relaxed S_1 after geometrical optimization using TD-DFT method in Gaussian (Section 2.4) [10], and the significant redshift from the FS emission peak wavelength is notable for the TICT state.

[c] The ϕ and ϕ' are defined as dihedral angles of the two N–CH_3 arms of –NMe_2 group with respect to the conjugated plane of compound **1** (see Figure 1a in main text). Notably, the dimethylamino group twists from a largely planar geometry (in FS) to perpendicular geometry (in TICT state), which indicates significant conformational motions of the dimethylamine in the excited state.

Table S4. Multivariable regression of nonradiative decay rate constant for compound **1**

Fitting formula	Coeff. [a]	k_{nr}		R^2
		value [b]	p-value [b]	
Eqn. (8)	a	0.68	0.0444	0.82
	b	1.27	0.0344	
	p	0.78	0.2109	
	δ [c]	0.61	0.2538	
	$\log(k_0)$	7.05	4.2×10^{-6}	
Eqn. (9)	e	1.84	0.0018	0.84
	δ [c]	–0.16	0.7082	
	$\log(k_0)$	7.63	2.6×10^{-8}	

[a] The logarithm of rate constant (unit of s^{-1}) is unitless, and the fit intercept $\log(k_0)$ is also unitless (see Equation (8) in main text).

[b] The statistically significant coefficients ($p \leq 0.05$) for the nonradiative decay rate constants of compound **1** in 11 solvents are highlighted by light orange shades. Both positive coefficients in Equation (8) (a and b) for solvent H-bonding parameters (α and β) as well as Equation (9) (e) for solvent polarity parameter (E_T^N) indicate that the strengthening of solvent H-bonding capabilities and/or polarity increases the solute chromophore's nonradiative decay rate constant and leads to a reduced FQY (see Figure 4 in main text).

[c] For the associated viscosity η value at 20 °C, it ranges from 0.32 cP in acetone, 0.37 cP in ACN, 0.43 cP in DCM, 0.46 cP in EtOAc, 0.55 cP in MeOH, 0.59 cP in toluene, 0.92 cP in DMF, 1.0 cP in water, 1.2 cP in EtOH, 1.37 cP in dioxane, and 2.4 cP in 2-PrOH. The unit of centipoise (cP) is 1 cP = 1×10^{-3} Pa·s. Given the logarithm base 10 of viscosity values in Eqn. 8 and 9 (main text), variation of the resulting numbers is relatively small, yet it ranges from negative (for $\eta < 1$) to positive values (for $\eta > 1$) and supports the multivariable analysis with a sufficiently large phase space [11] to confirm a negligible dependence of dimethylamine isomerization rate on viscosity.

4. References

(1) Samih, F.; Prudhomme, M.; Dauphin, G.; Jeminet, G. Semi-synthesis of A.23187 (calcimycin) analogs with 5-n-amino substituents. Their complexation of calcium and magnesium. *Tetrahedron* **1990**, *46*, 5177–5186.

(2) Rauckman, B.S.; Tidwell, M.Y.; Johnson, J.V.; Roth, B. 2, 4-Diamino-5-benzylpyrimidines and analogs as antibacterial agents. 10. 2, 4-Diamino-5-(6-quinolylmethyl)-and-[(tetrahydro-6-quinolyl)methyl] pyrimidine derivatives. Further specificity studies. *J. Med. Chem.* **1989**, *32*, 1927–1935.

(3) Šilhánková, A.; Ferles, M.; Malý, J. Some reactions of 6-formyl-1-methyl-1,2,3,4-tetrahydroquinoline. *Collect. Czech. Chem. Commun.* **1978**, *43*, 1484–1487.

(4) Hori, M.; Watanabe, I.; Ohtaka, H.; Harada, K.; Maruo, J.; Morita, T.; Yamamoto, T.; Tsutsui, H. US5597820A: 1,4-benzoxazine derivative and pharmaceutical compositions containing the same; Akzo Nobel NV: United States, **1997**.

(5) Walker, D.P.; Wishka, D.G.; Piotrowski, D.W.; Jia, S.; Reitz, S.C.; Yates, K.M.; Myers, J.K.; Vetman, T.N.; Margolis, B.J.; Jacobsen, E.J.; et al. Design, synthesis, structure–activity relationship, and in vivo activity of azabicyclic aryl amides as α7 nicotinic acetylcholine receptor agonists. *Bioorg. Med. Chem.* **2006**, *14*, 8219–8248.

(6) Snellenburg, J.J.; Laptenok, S.P.; Seger, R.; Mullen, K.M.; van Stokkum, I.H.M. Glotaran: A Java-based graphical user interface for the R-package TIMP. *J. Stat. Softw.* **2012**, *49*, 1–22.

(7) Fang, C.; Tang, L.; Chen, C. Unveiling coupled electronic and vibrational motions of chromophores in condensed phases. *J. Chem. Phys.* **2019**, *151*, 200901.

(8) Kamlet, M.J.; Abboud, J.-L.M.; Abraham, M.H.; Taft, R.W. Linear solvation energy relationships. 23. A comprehensive collection of the solvatochromic parameters, π*, α, and β, and

some methods for simplifying the generalized solvatochromic equation. *J. Org. Chem.* **1983**, *48*, 2877–2887.

(9) Chen, C.; Baranov, M.S.; Zhu, L.; Baleeva, N.S.; Smirnov, A.Y.; Zaitseva, S.; Yampolsky, I.V.; Solntsev, K.M.; Fang, C. Designing redder and brighter fluorophores by synergistic tuning of ground and excited states. *Chem. Commun.* **2019**, *55*, 2537–2540.

(10) Frisch, M.J.; Trucks, G.W.; Schlegel, H.B.; Scuseria, G.E.; Robb, M.A.; Cheeseman, J.R.; Scalmani, G.; Barone, V.; Petersson, G.A.; Nakatsuji, H.; et al. *Gaussian 16, Rev. C.01*; Gaussian, Inc.: Wallingford, CT, 2016.

(11) Chen, C.; Tachibana, S.R.; Baleeva, N.S.; Myasnyanko, I.N.; Bogdanov, A.M.; Gavrikov, A.S.; Mishin, A.S.; Malyshevskaya, K.K.; Baranov, M.S.; Fang, C. Developing bright green fluorescent protein (GFP)-like fluorogens for live-cell imaging with nonpolar protein−chromophore interactions. *Chem. Eur. J.* **2021**, *27*, 8946–8950.

5. Supplementary NMR Spectra (S1–S26)

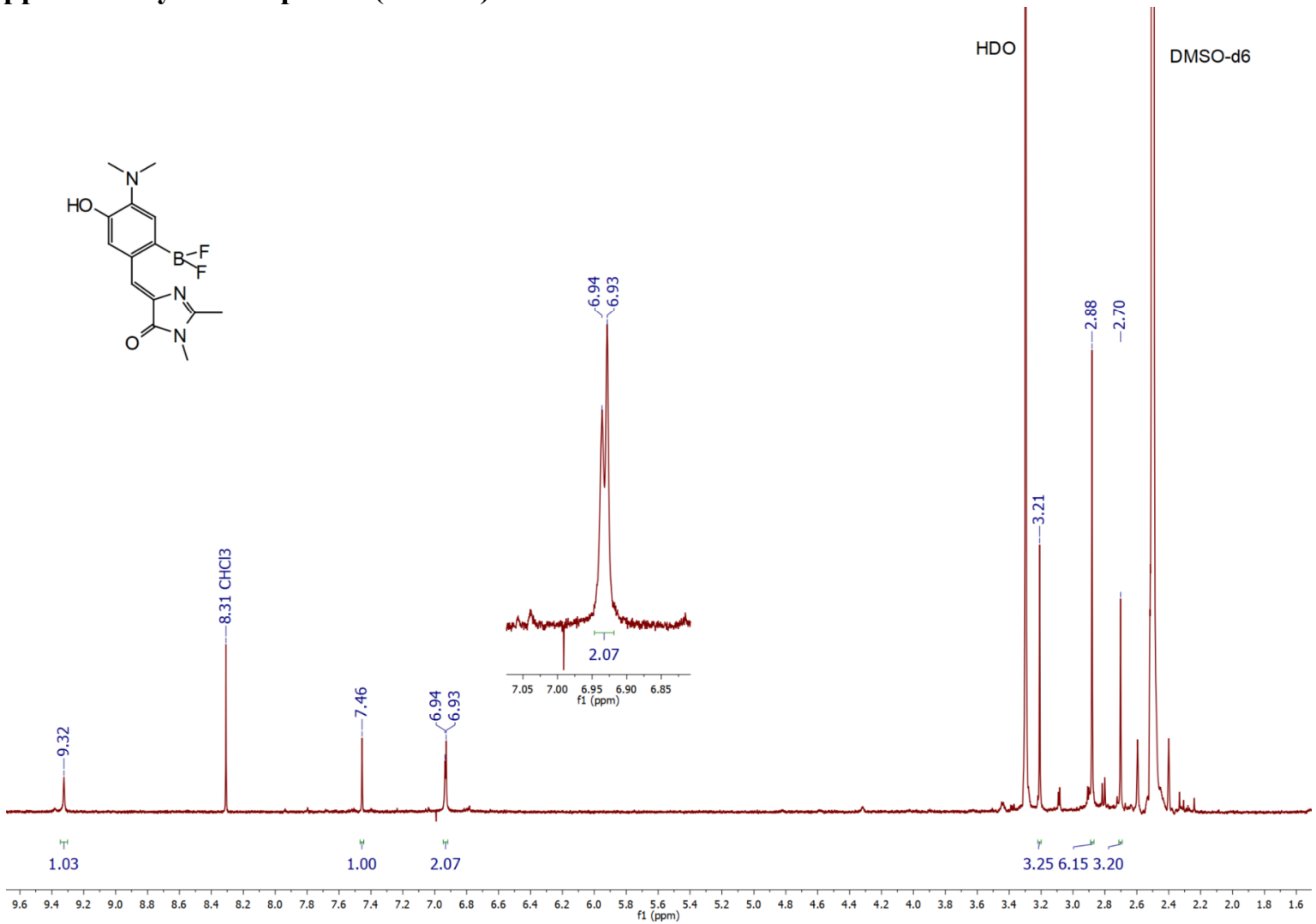

Supplementary S1. ^{1}H NMR spectrum of compound **1**.

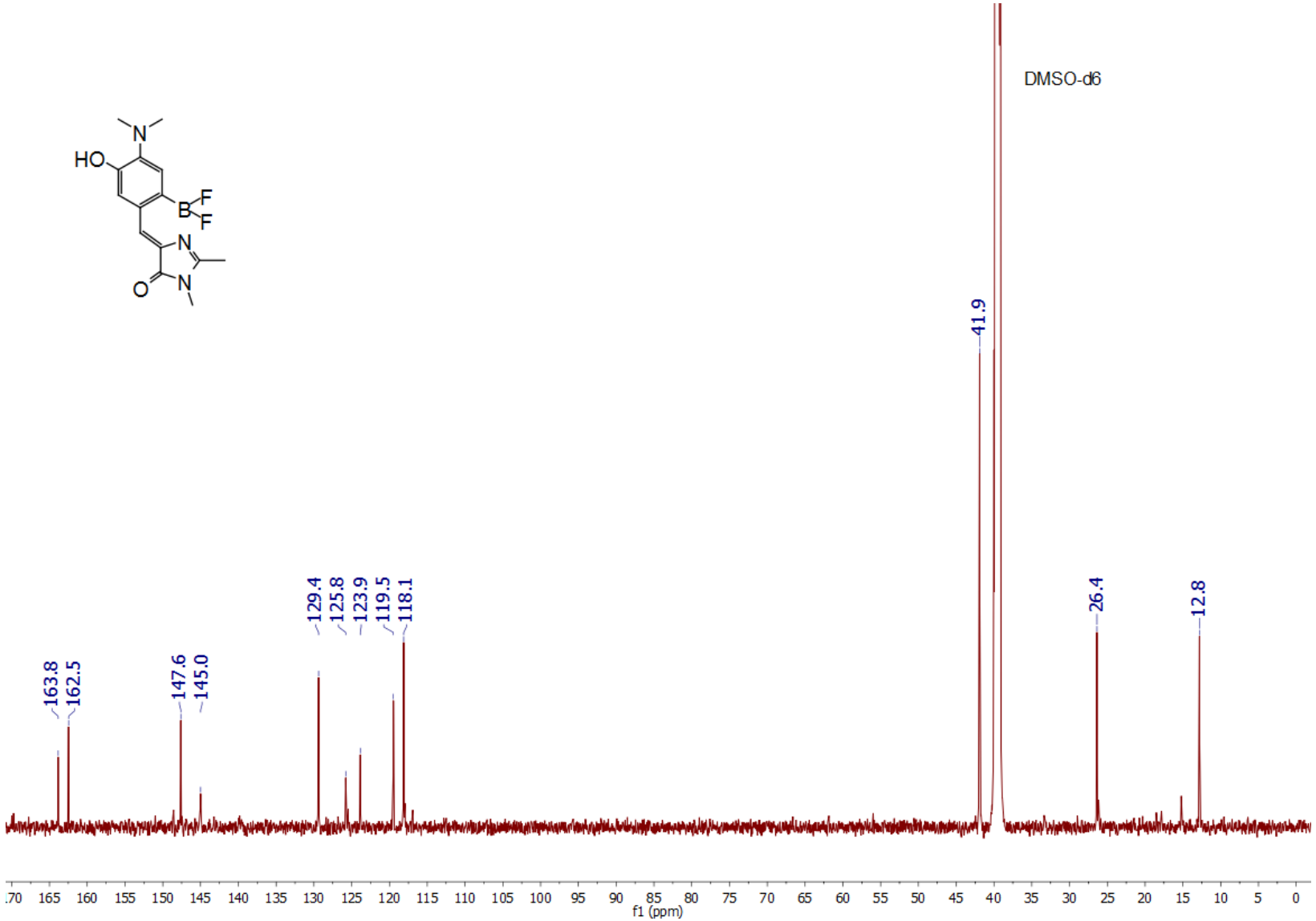

Supplementary S2. ^{13}C NMR spectrum of compound **1**.

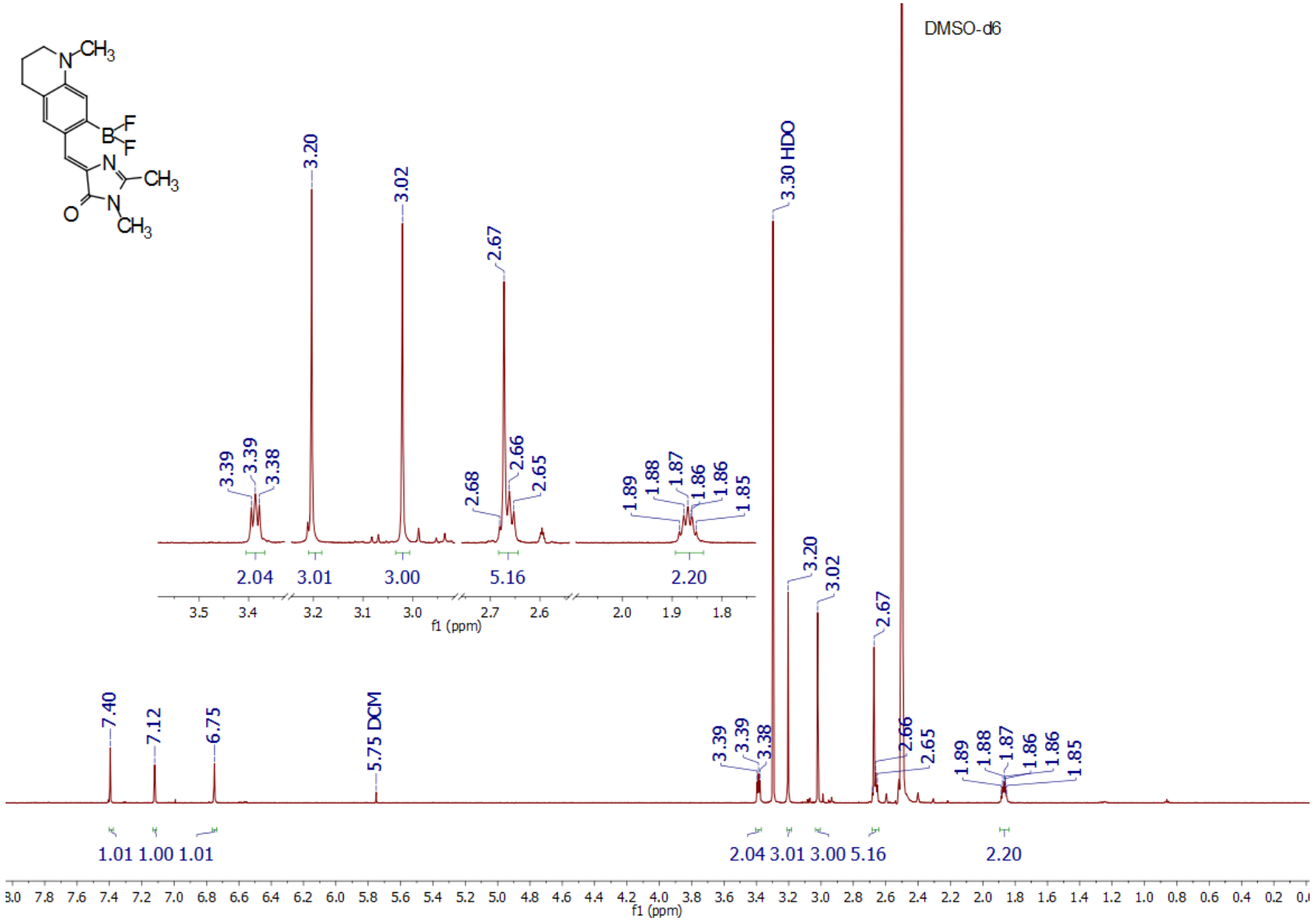

Supplementary S3. [1]H NMR spectrum of compound **2**.

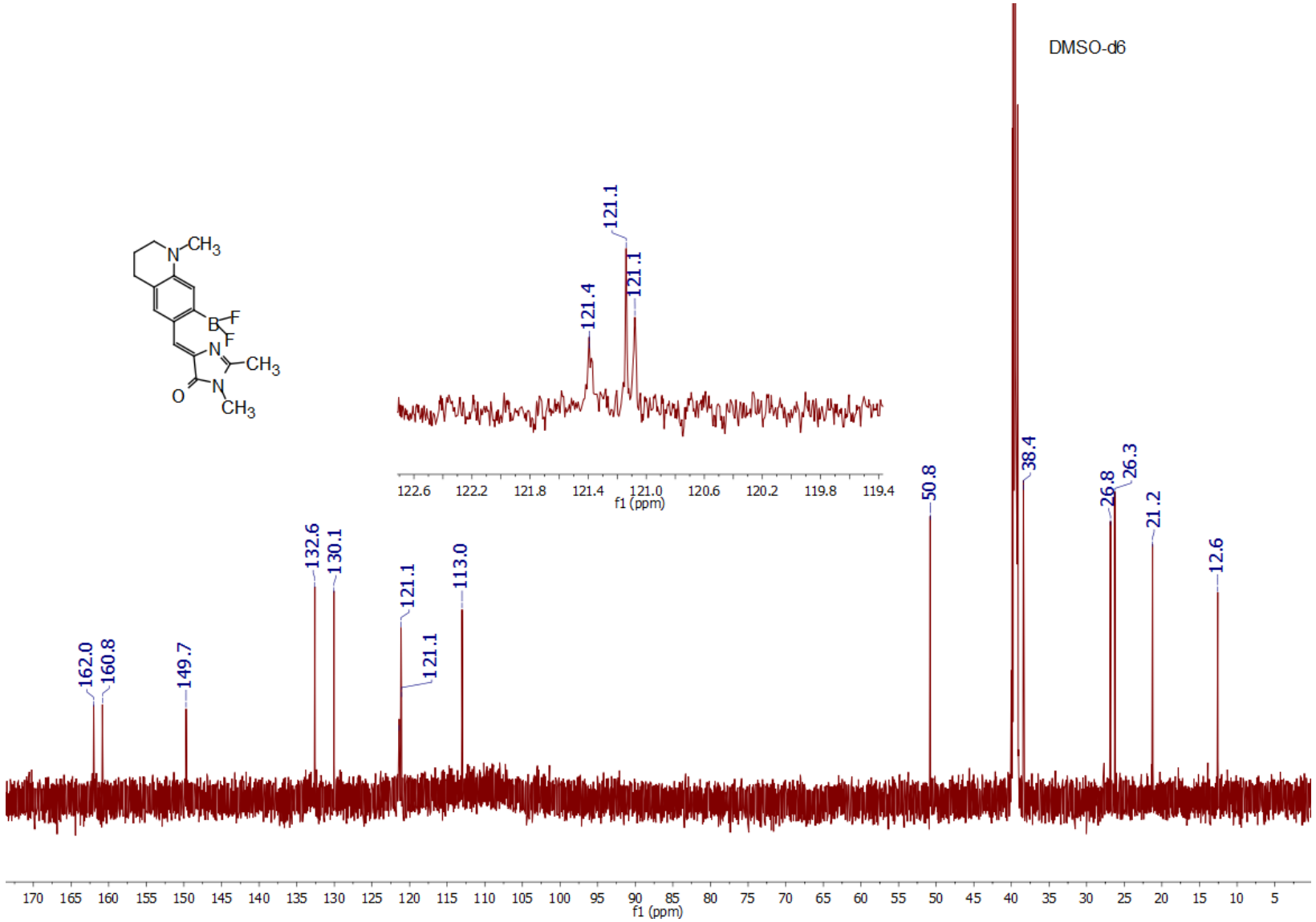

Supplementary S4. ^{13}C NMR spectrum of compound **2**.

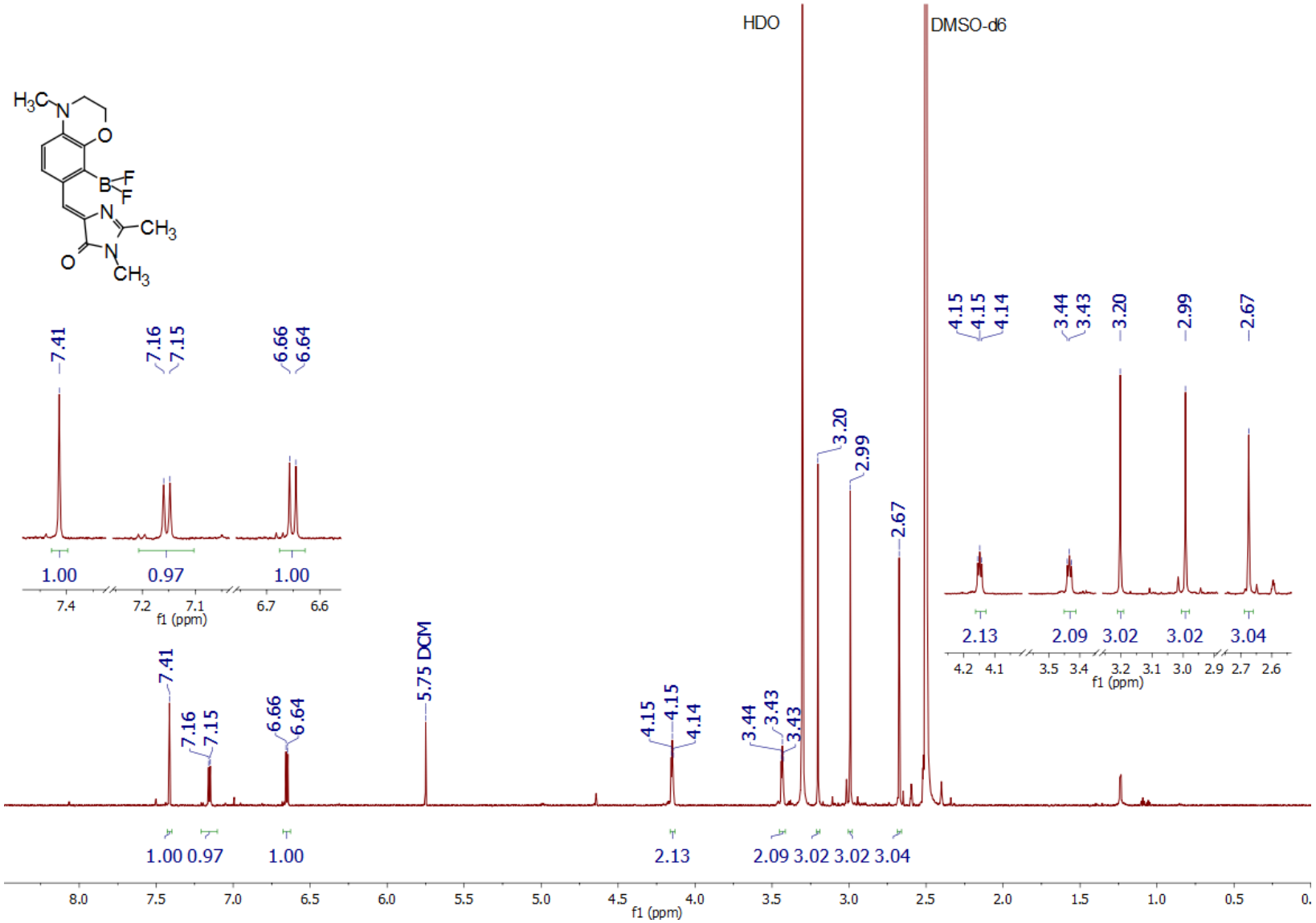

Supplementary S5. [1]H NMR spectrum of compound **3**.

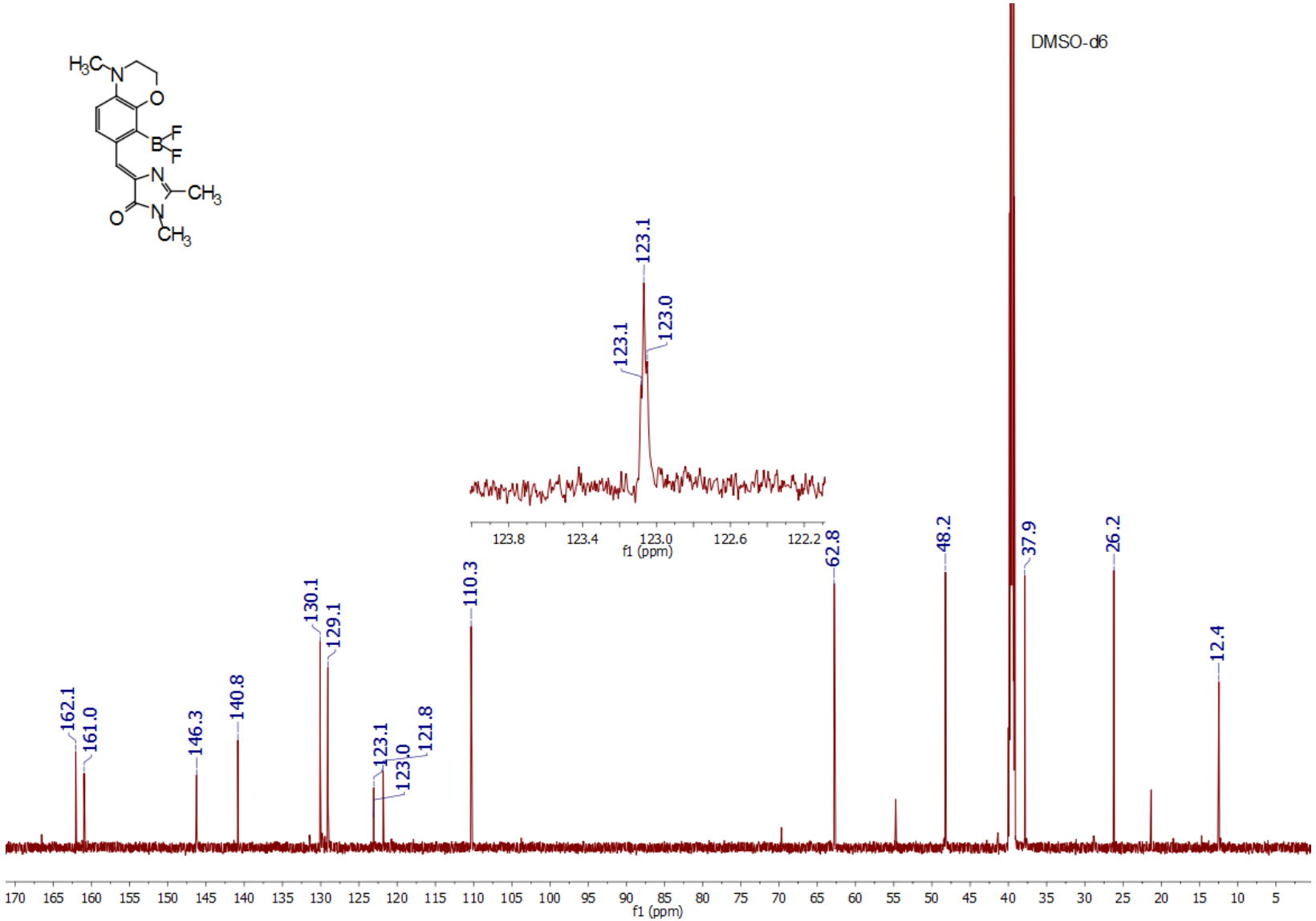

Supplementary S6. ^{13}C NMR spectrum of compound **3**.

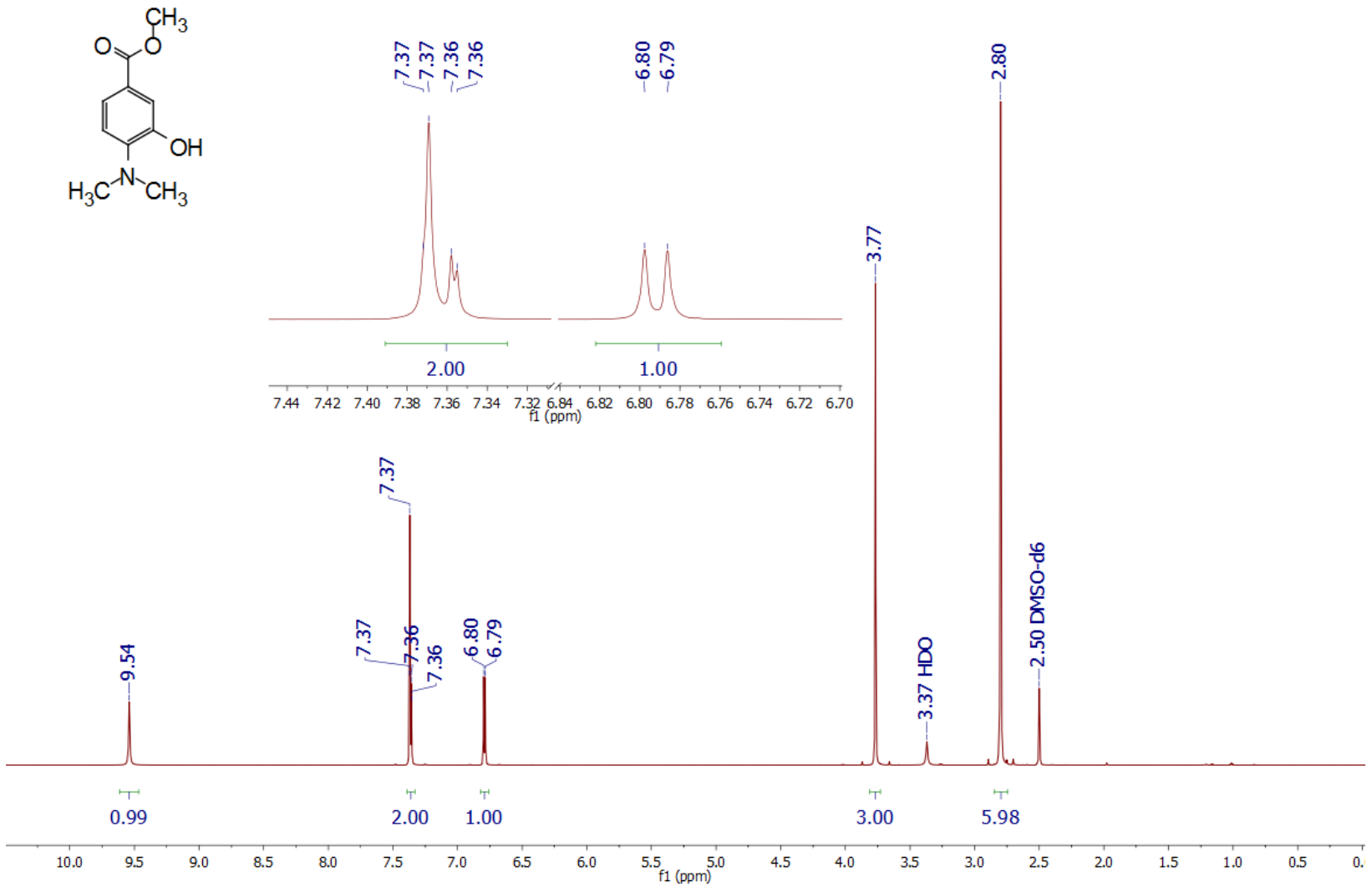

Supplementary S7. ^{1}H NMR spectrum of **SAI145** for synthesis of compound **1**.

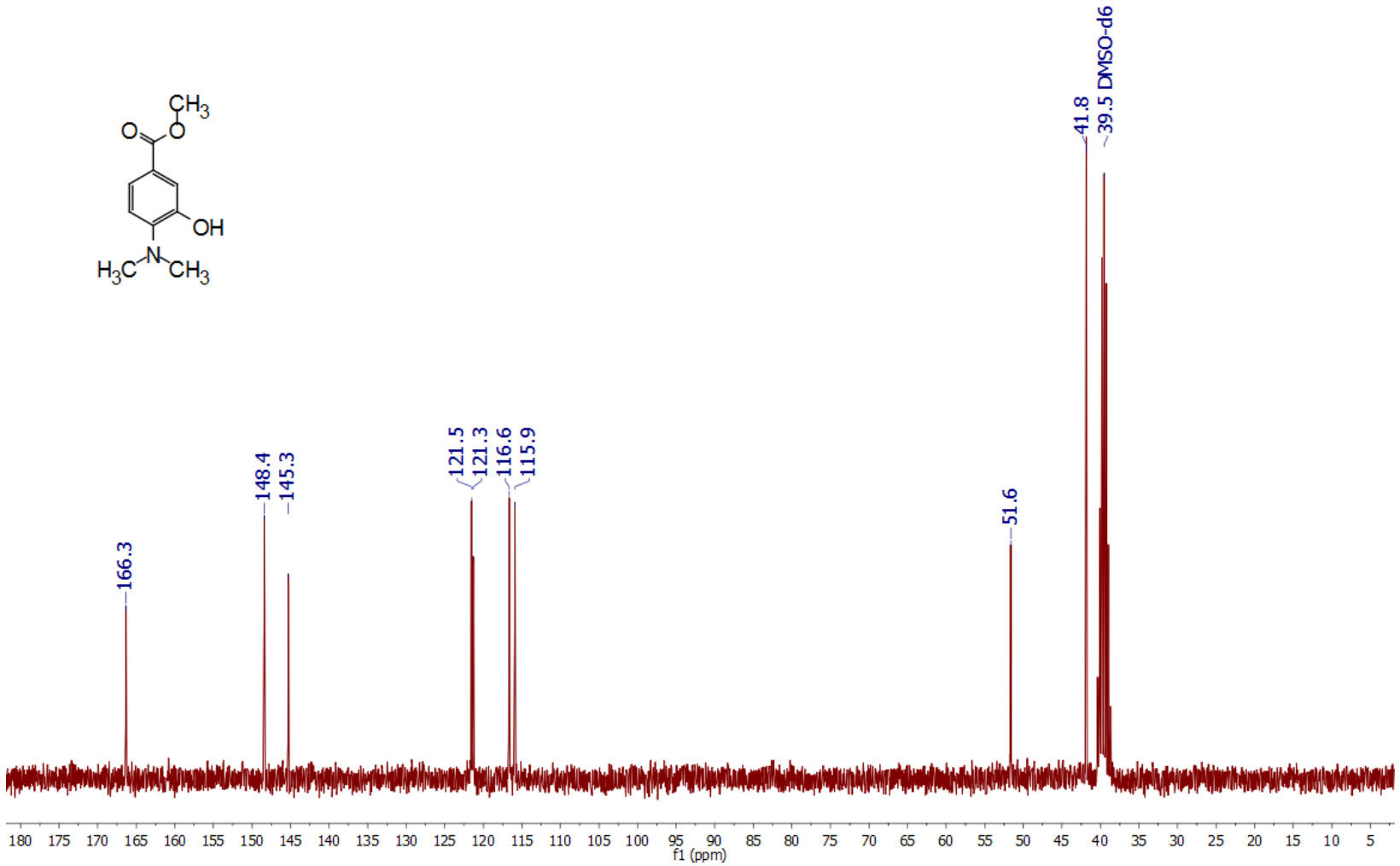

Supplementary S8. ^{13}C NMR spectrum of **SAI145** for synthesis of compound **1**.

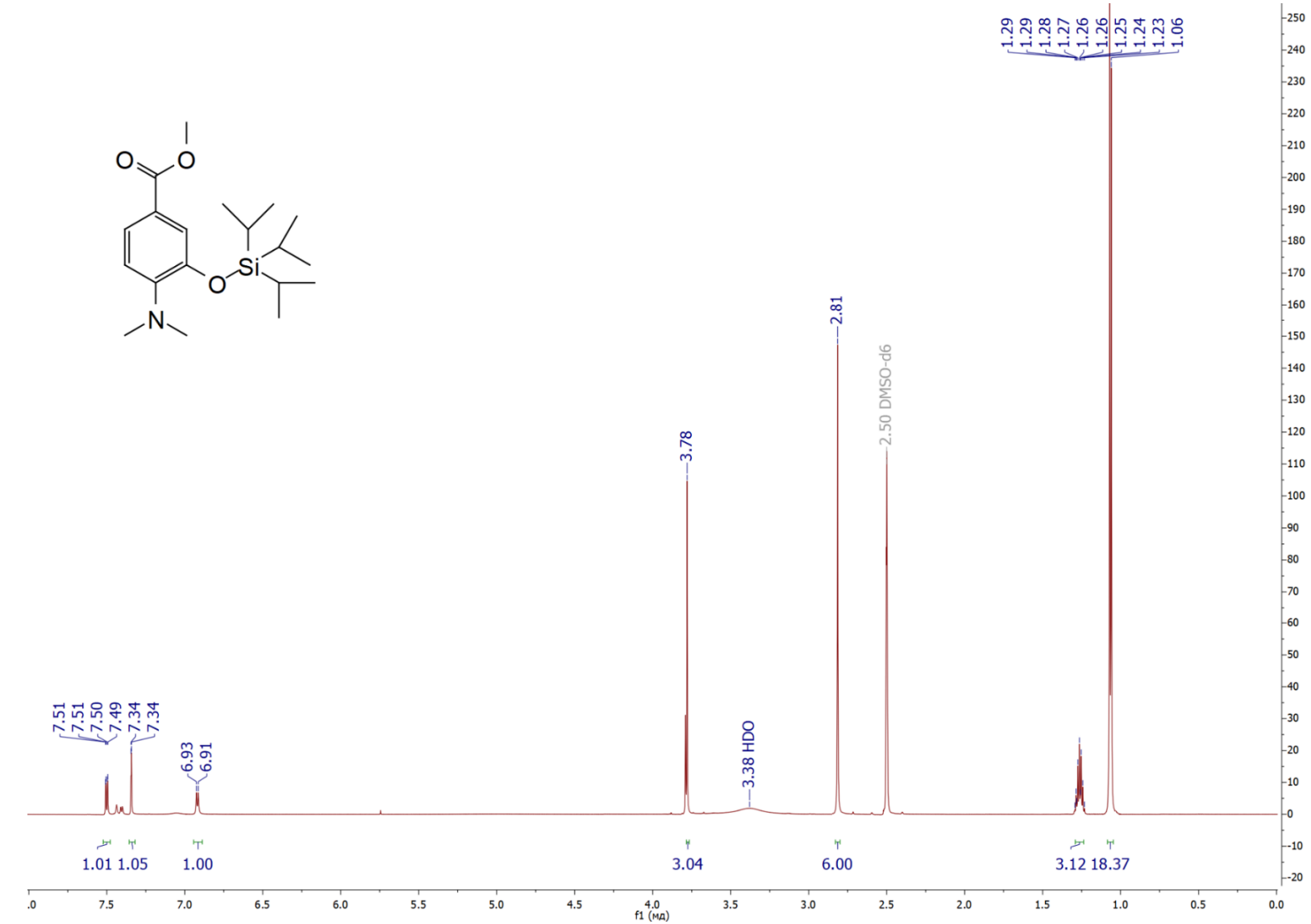

Supplementary S9. ^{1}H NMR spectrum of **SAI146** for synthesis of compound **1**.

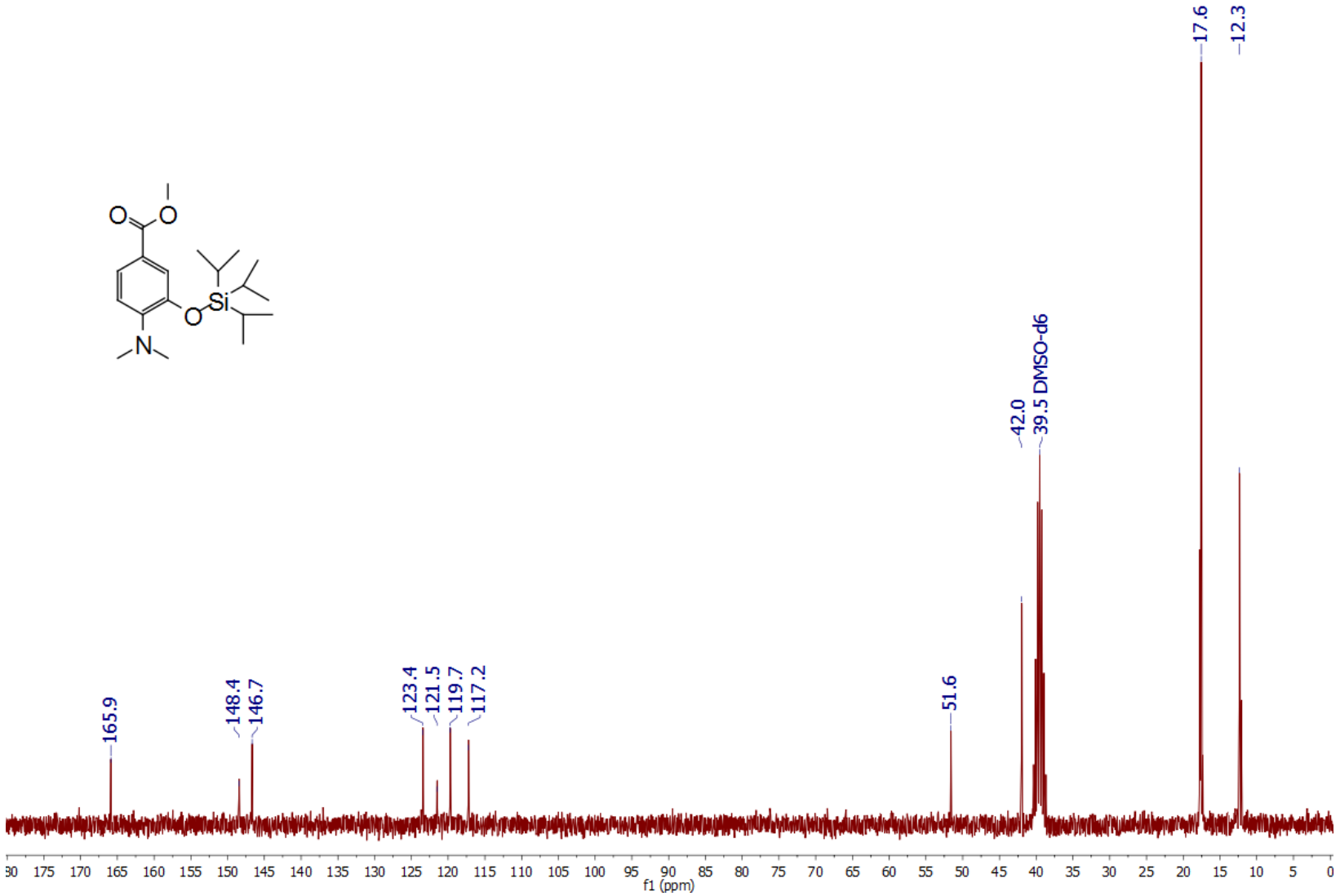

Supplementary S10. ^{13}C NMR spectrum of **SAI146** for synthesis of compound **1**.

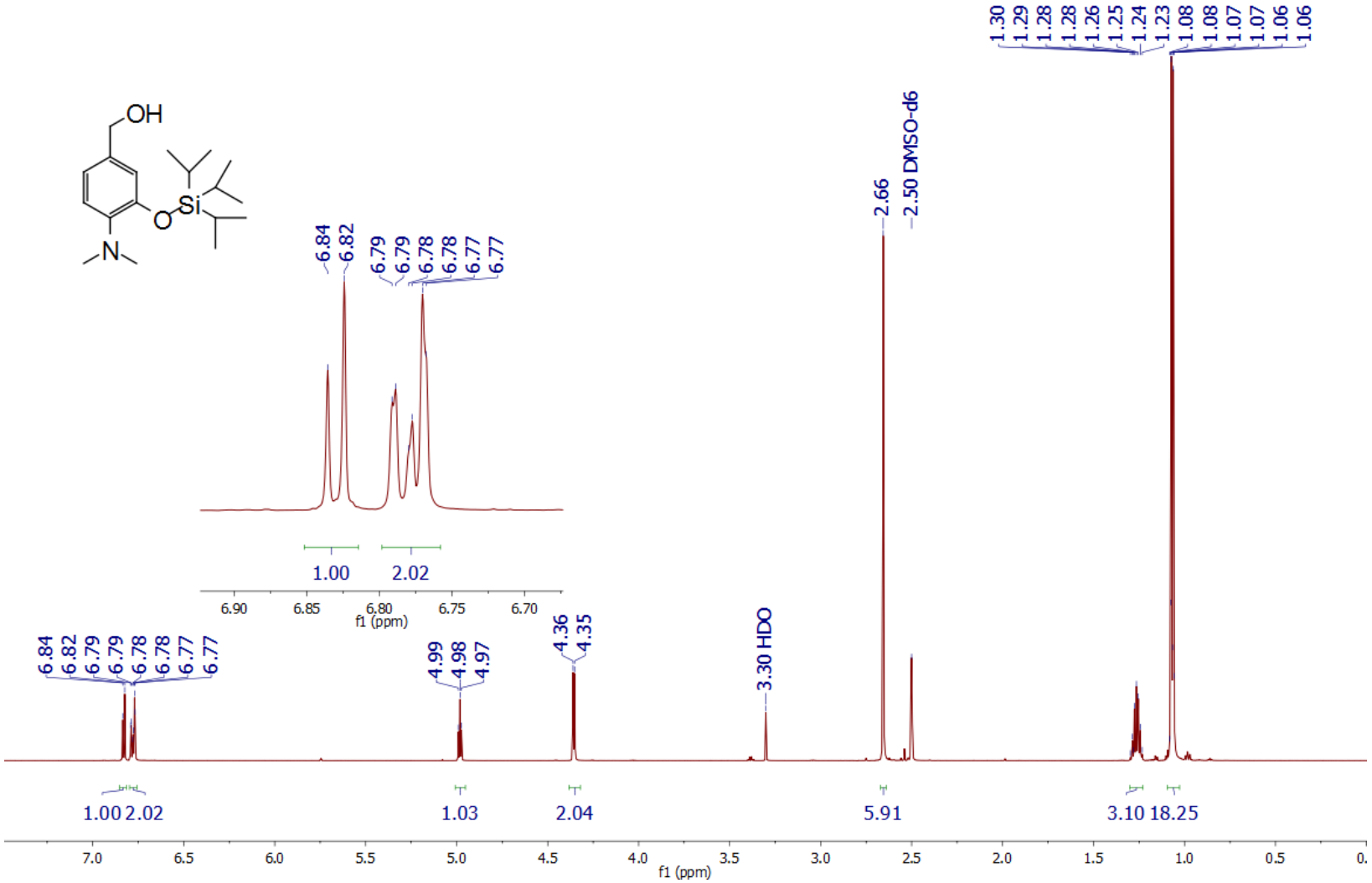

Supplementary S11. ^{1}H NMR spectrum of **SAI150** for synthesis of compound **1**.

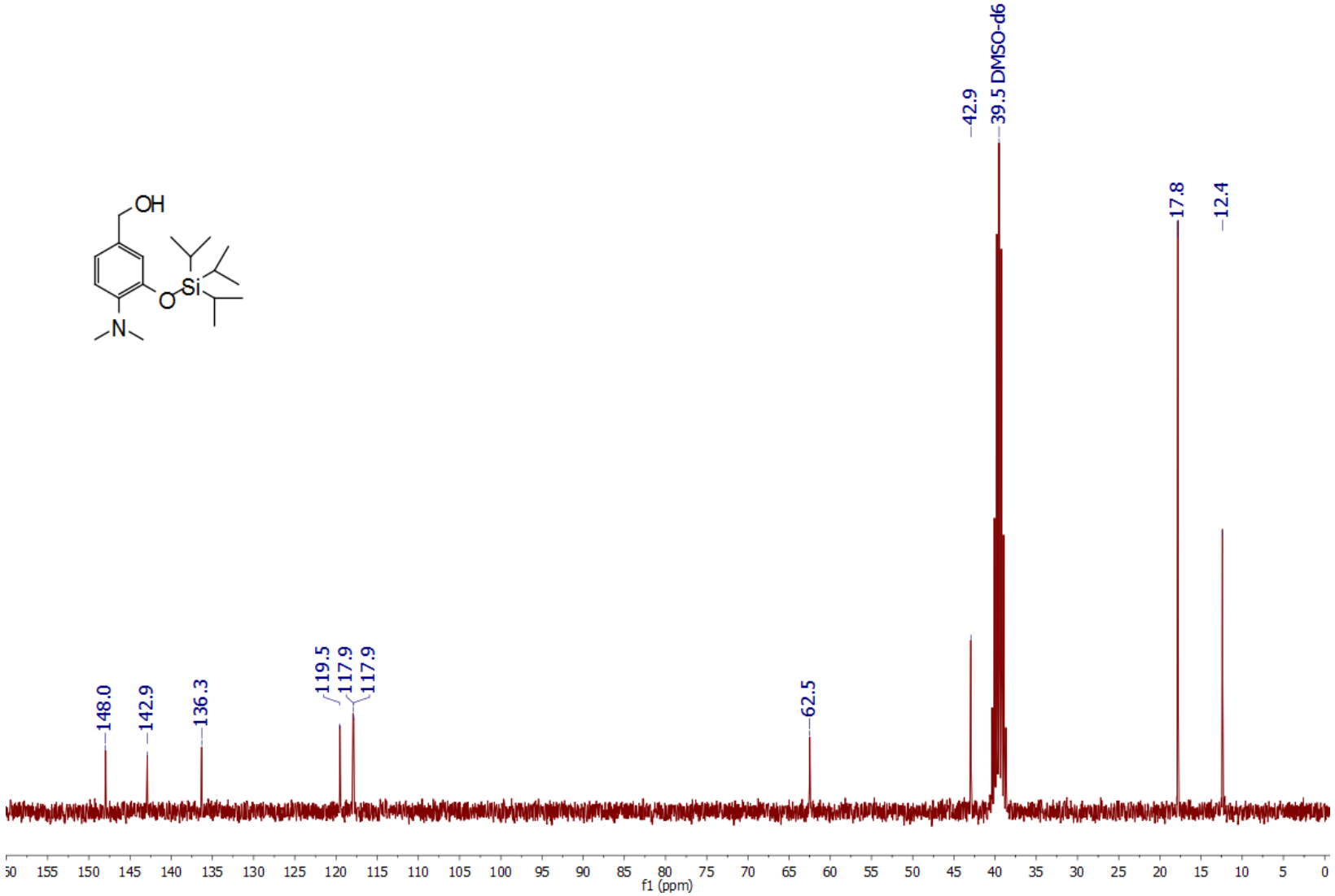

Supplementary S12. ^{13}C NMR spectrum of **SAI150** for synthesis of compound **1**.

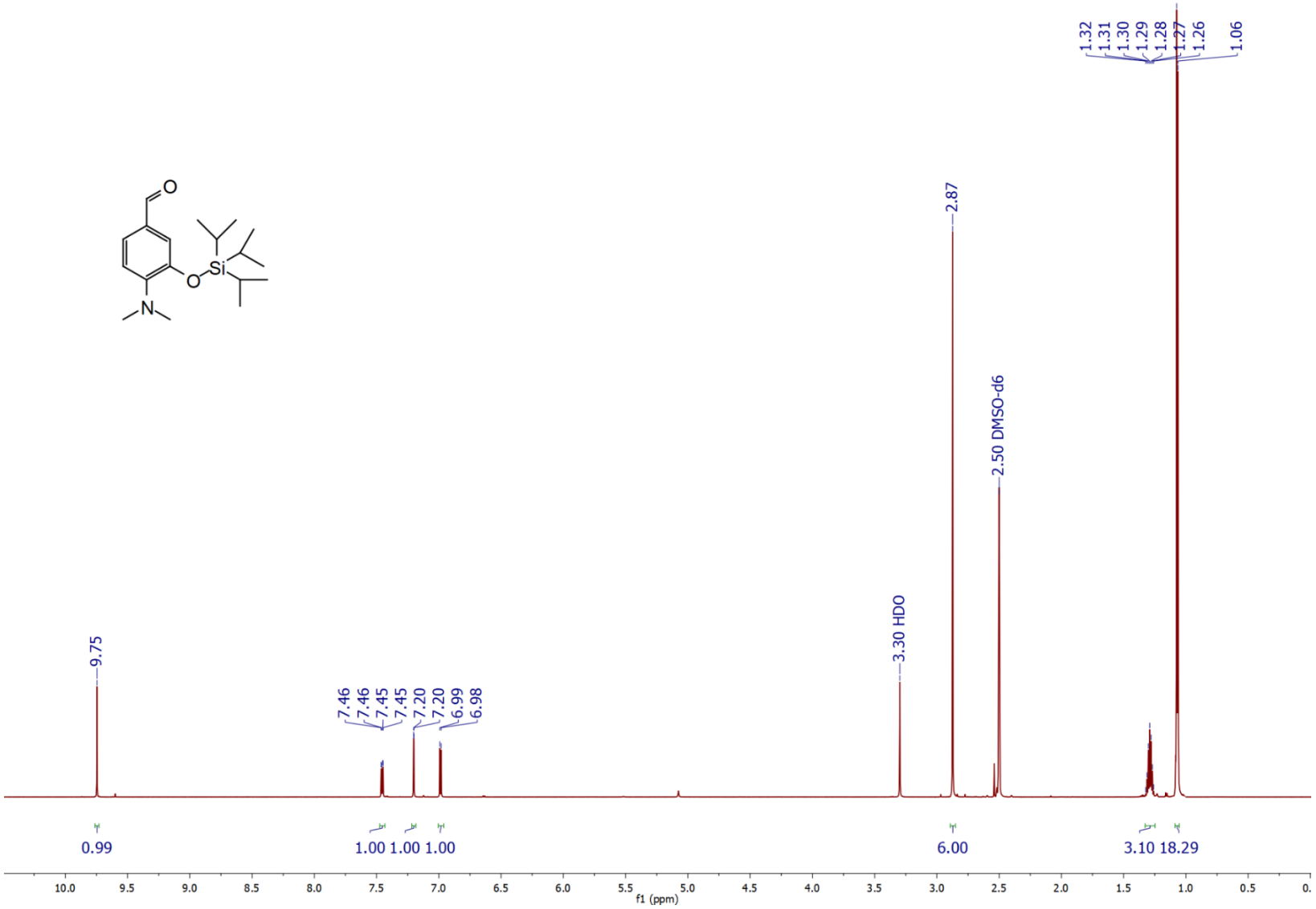

Supplementary S13. ^{1}H NMR spectrum of **SAI157** for synthesis of compound **1**.

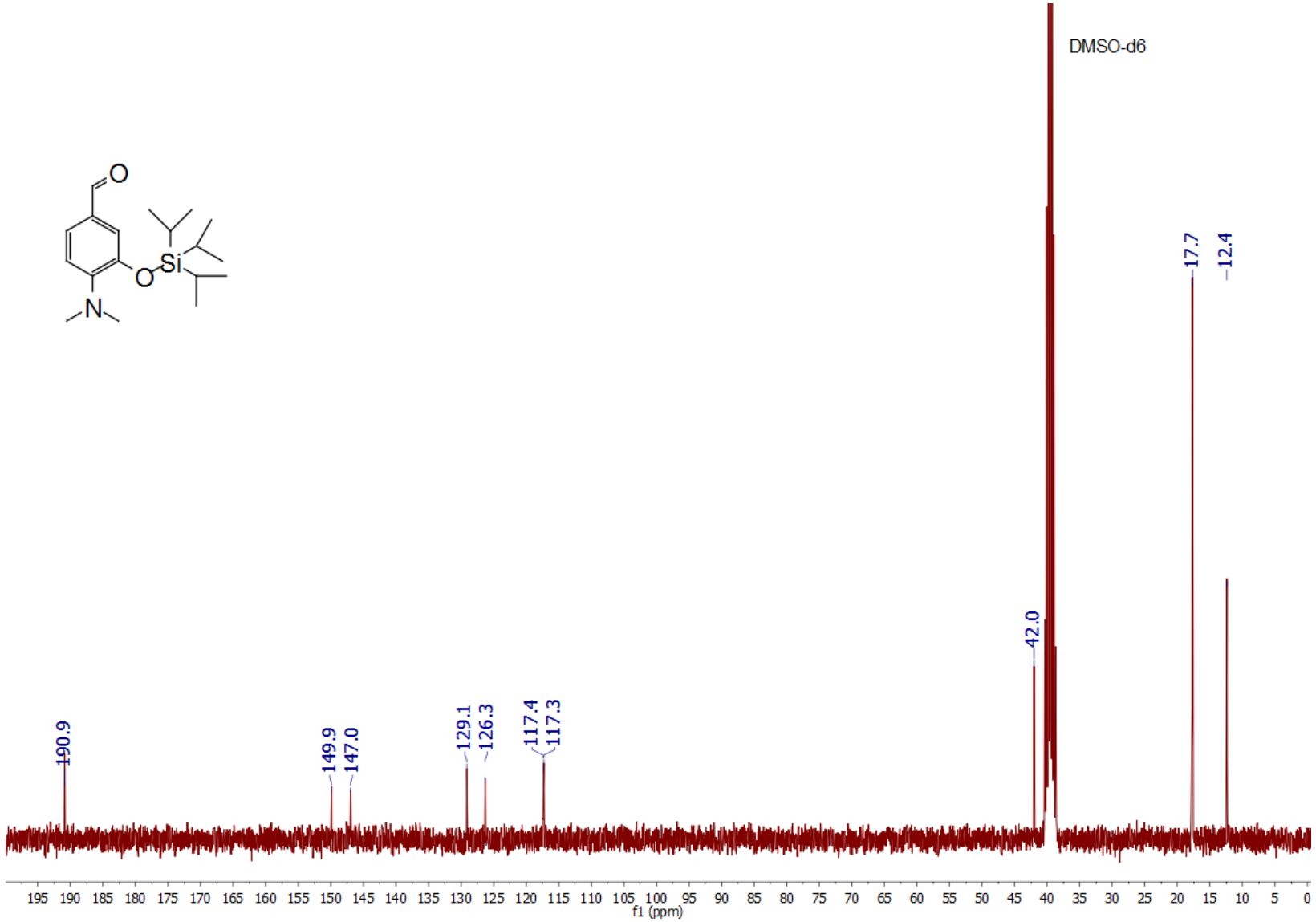

Supplementary S14. ^{13}C NMR spectrum of **SAI157** for synthesis of compound **1**.

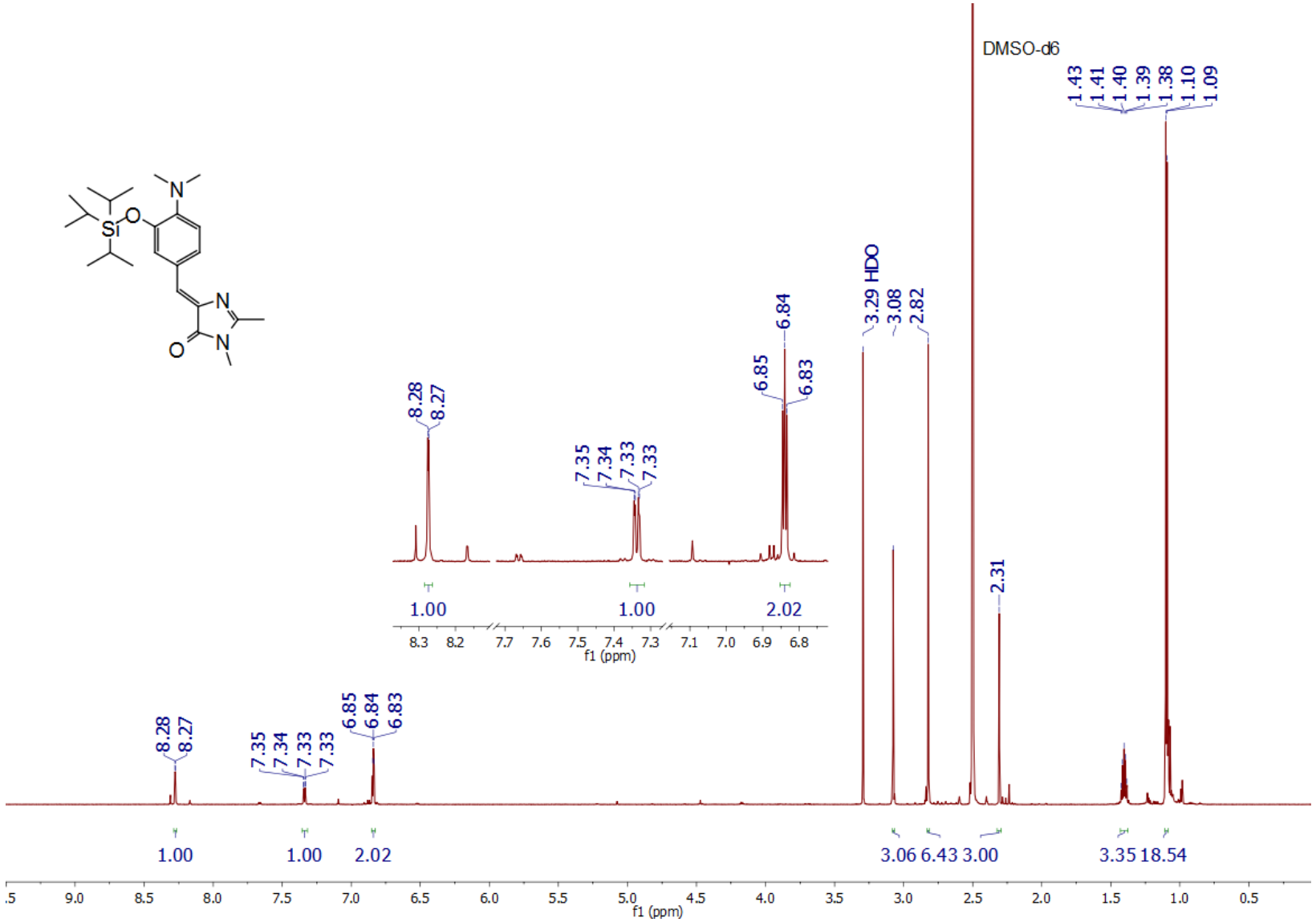

Supplementary S15. ^{1}H NMR spectrum of **SAI162** for synthesis of compound **1**.

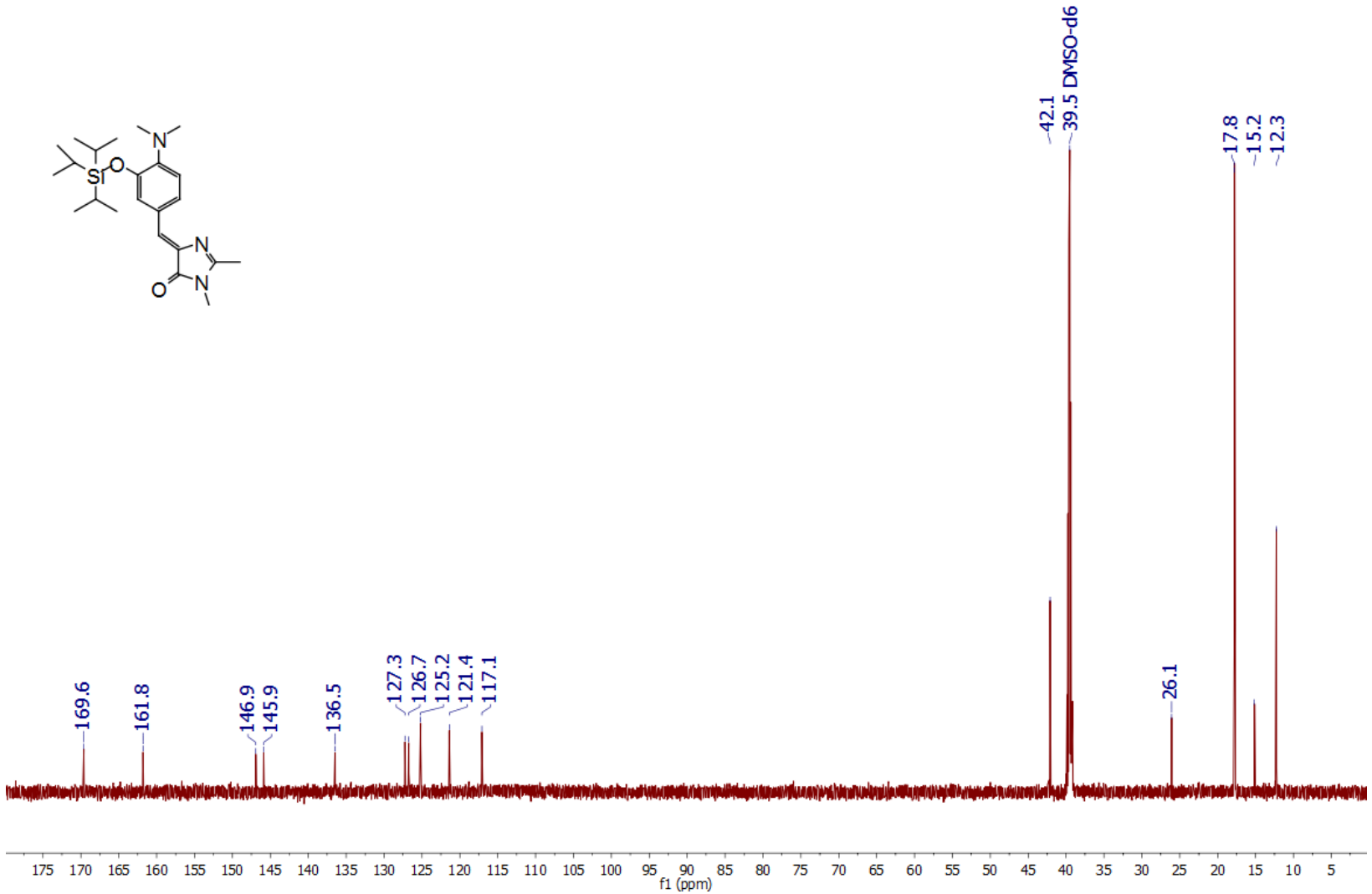

Supplementary S16. ^{13}C NMR spectrum of **SAI162** for synthesis of compound **1**.

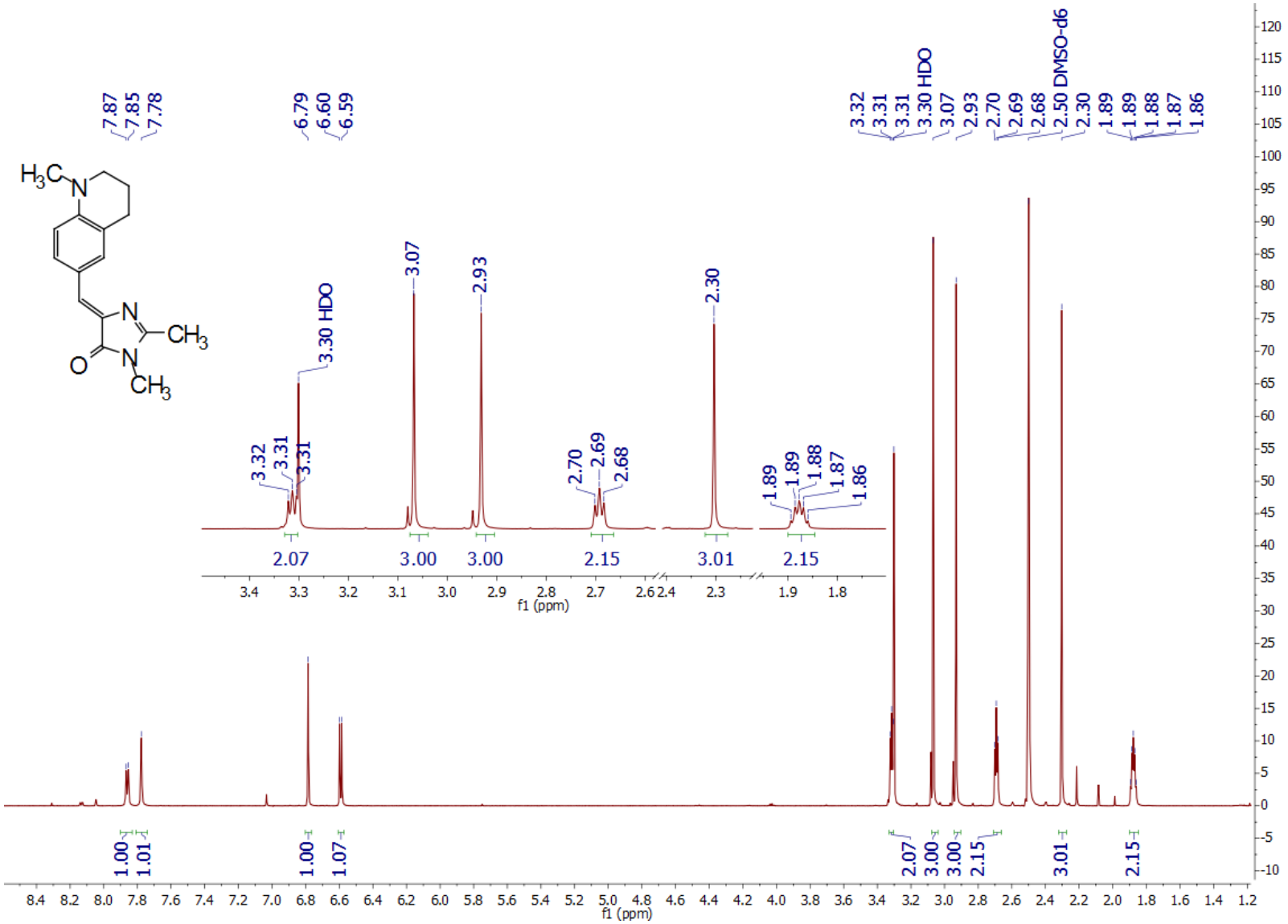

Supplementary S17. ^{1}H NMR spectrum of **SAI295** for synthesis of compound **2**.

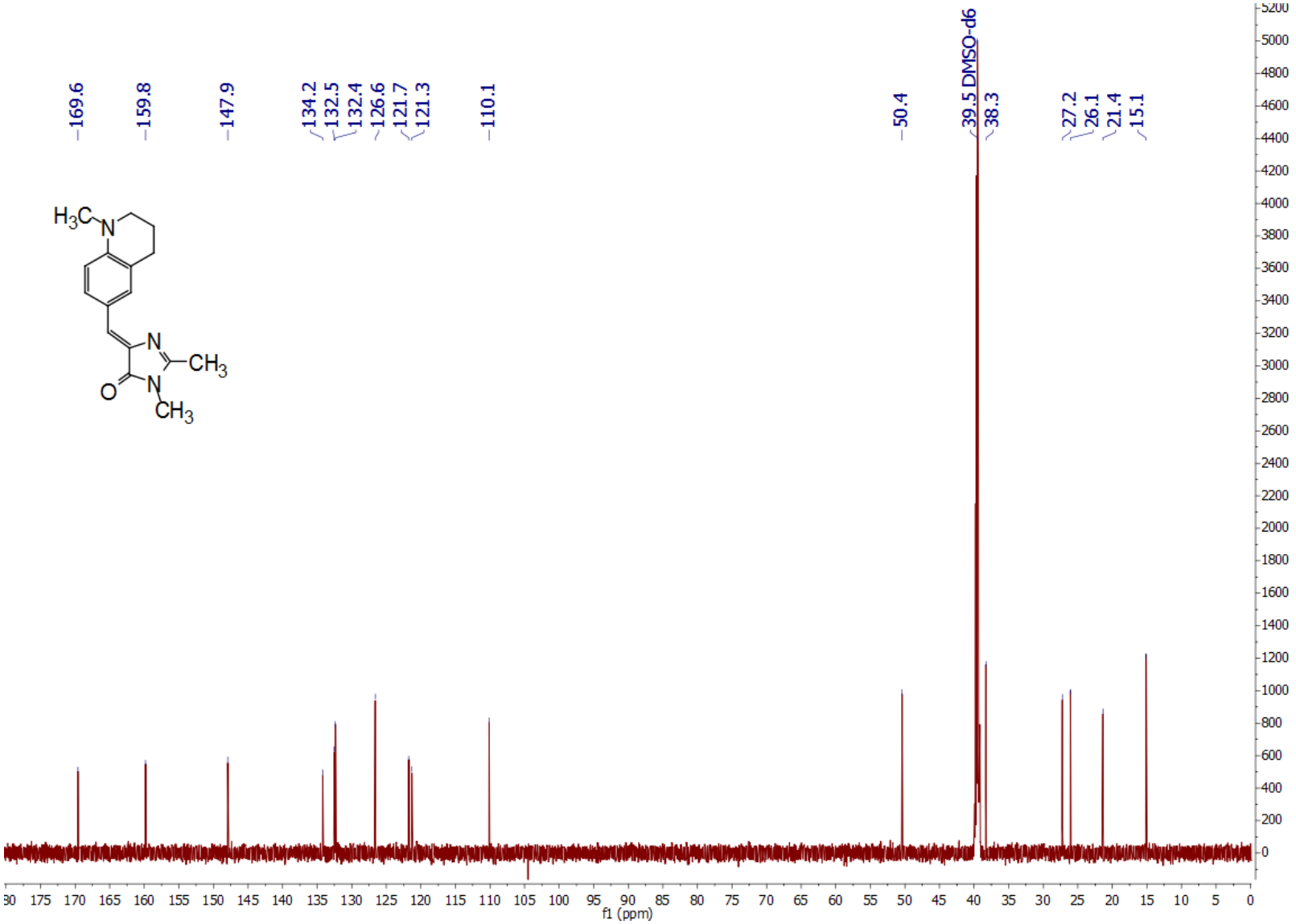

Supplementary S18. ^{13}C NMR spectrum of **SAI295** for synthesis of compound **2**.

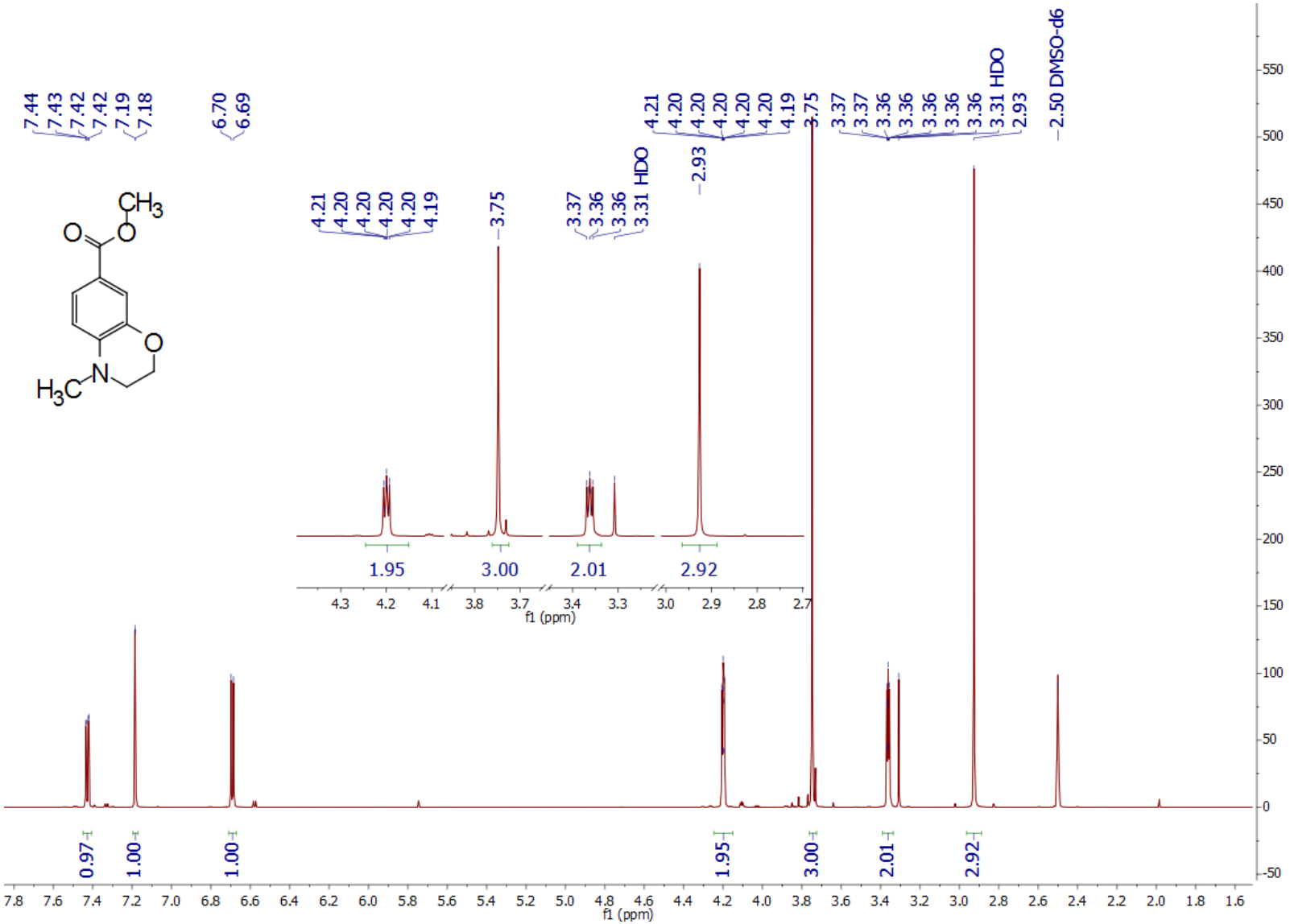

Supplementary S19. ^{1}H NMR spectrum of **SAI315** for synthesis of compound **3**.

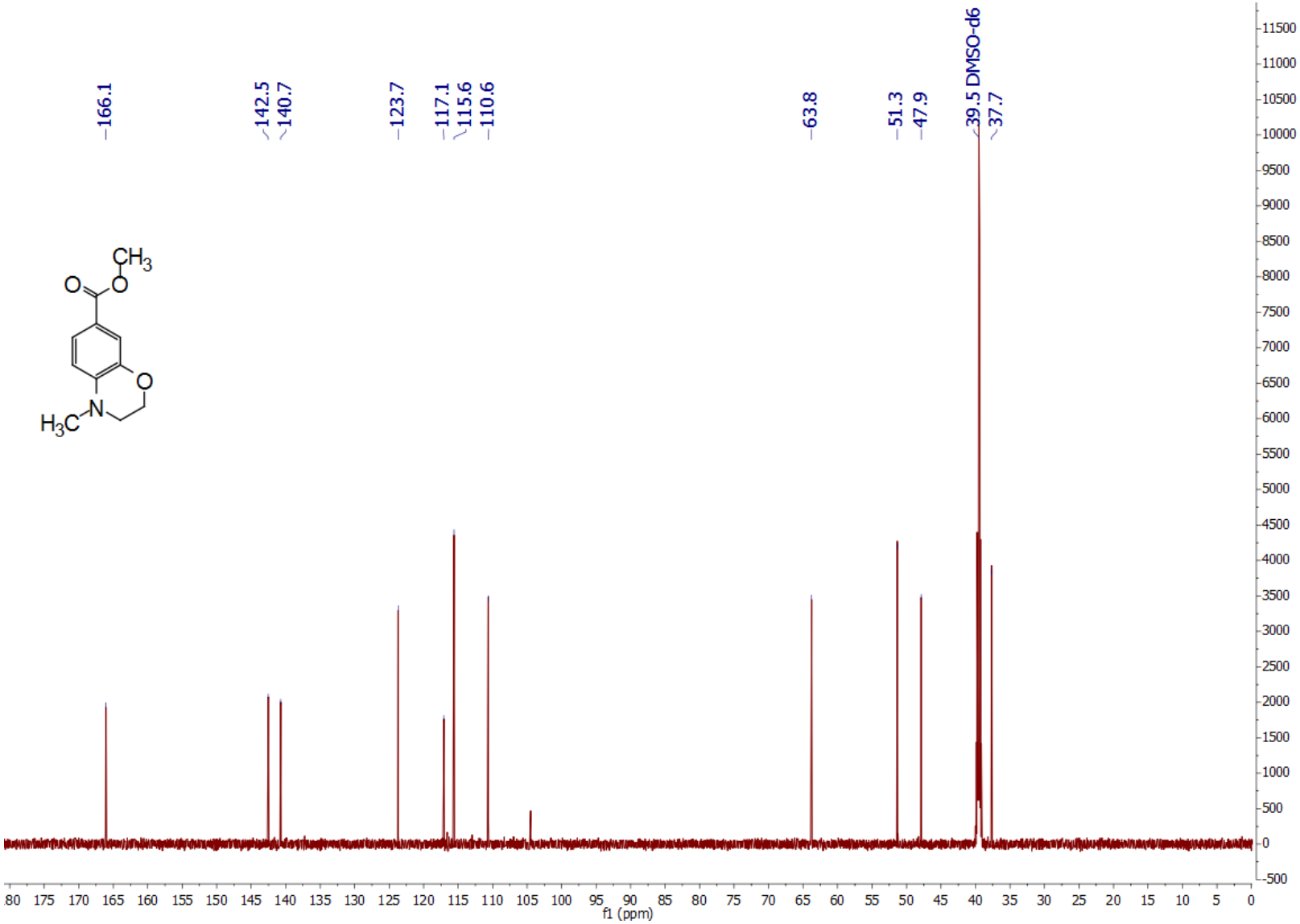

Supplementary S20. ^{13}C NMR spectrum of **SAI315** for synthesis of compound **3**.

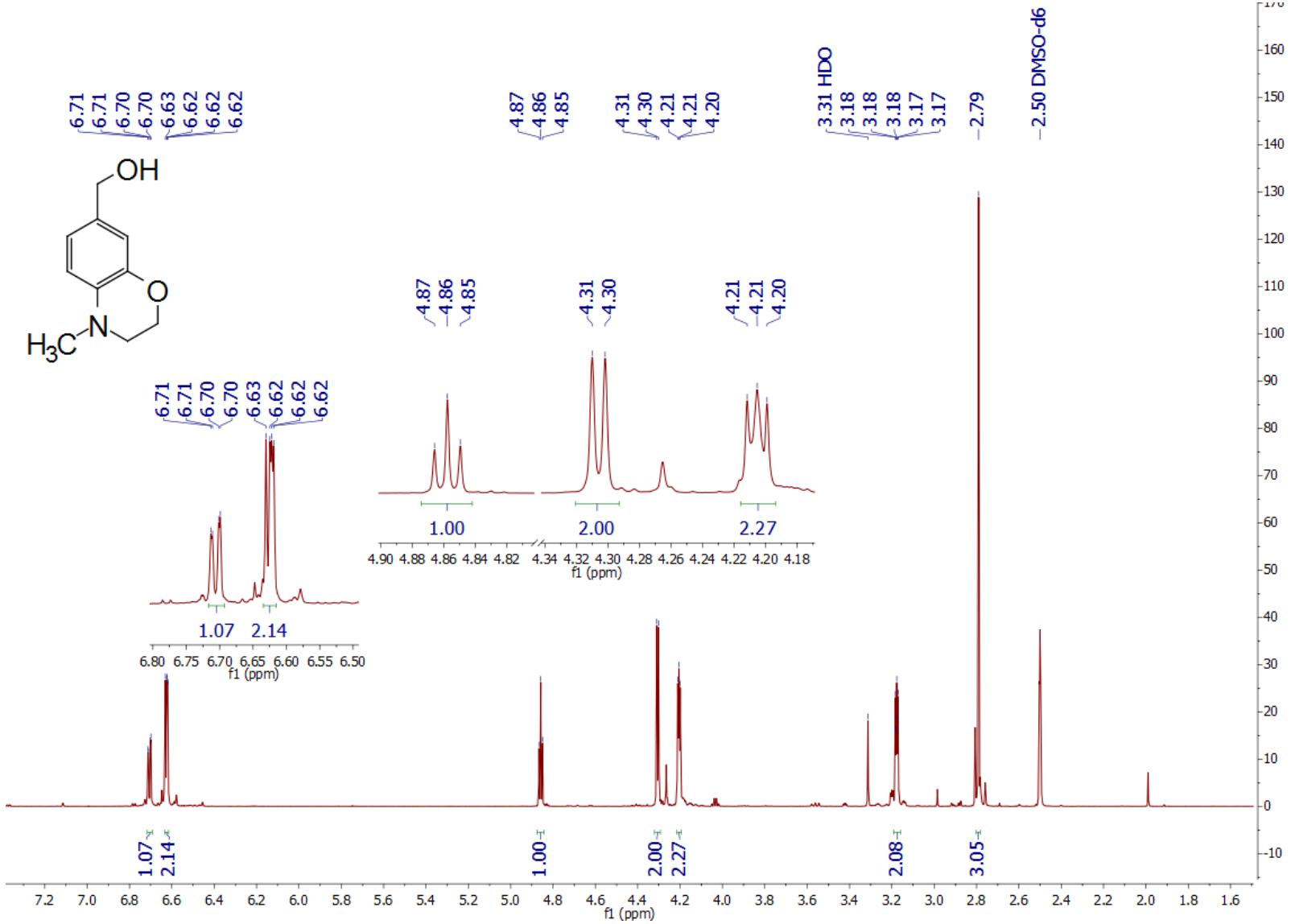

Supplementary S21. [1]H NMR spectrum of **SAI319** for synthesis of compound **3**.

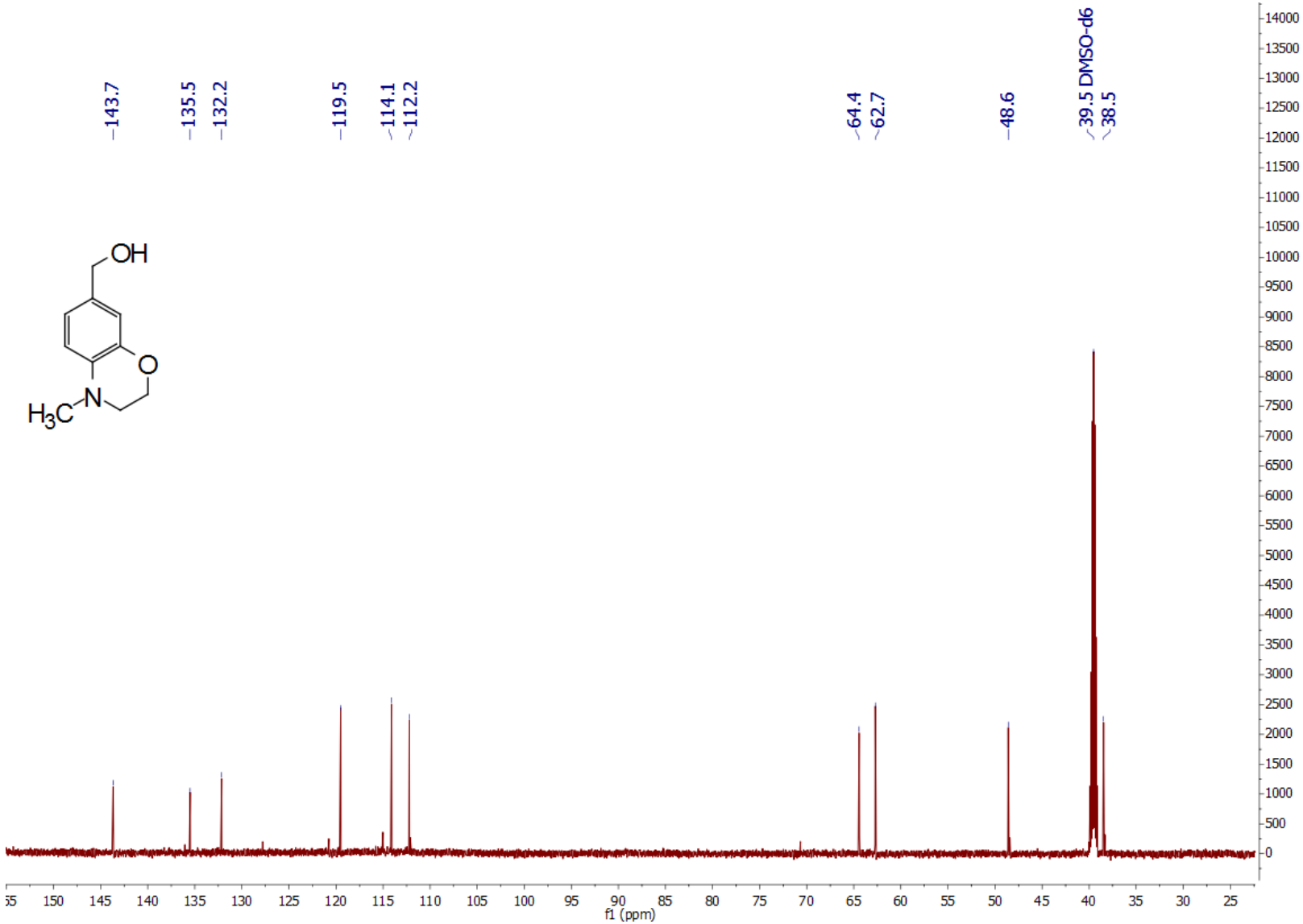

Supplementary S22. ^{13}C NMR spectrum of **SAI319** for synthesis of compound **3**.

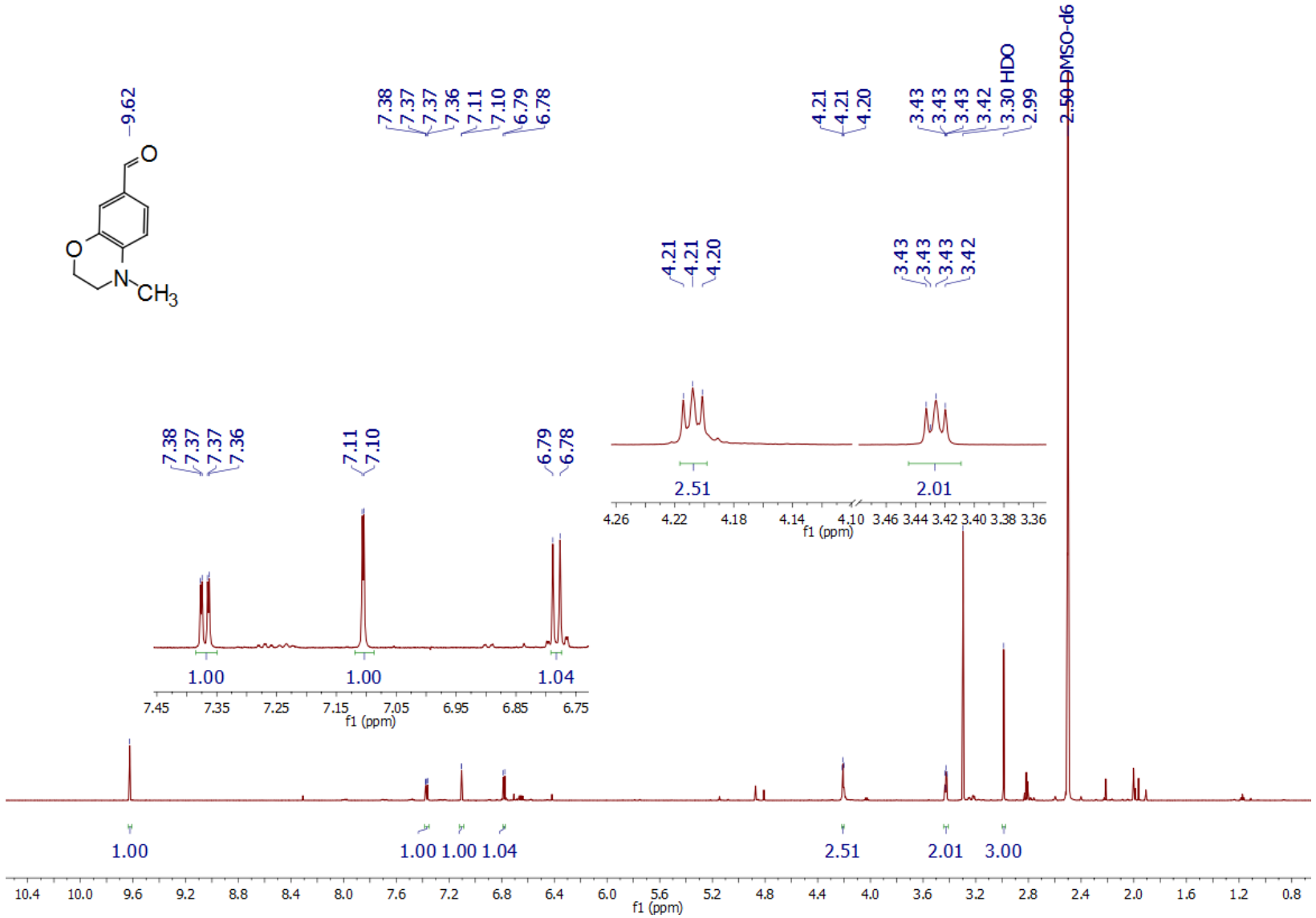

Supplementary S23. [1]H NMR spectrum of **SAI322** for synthesis of compound **3**.

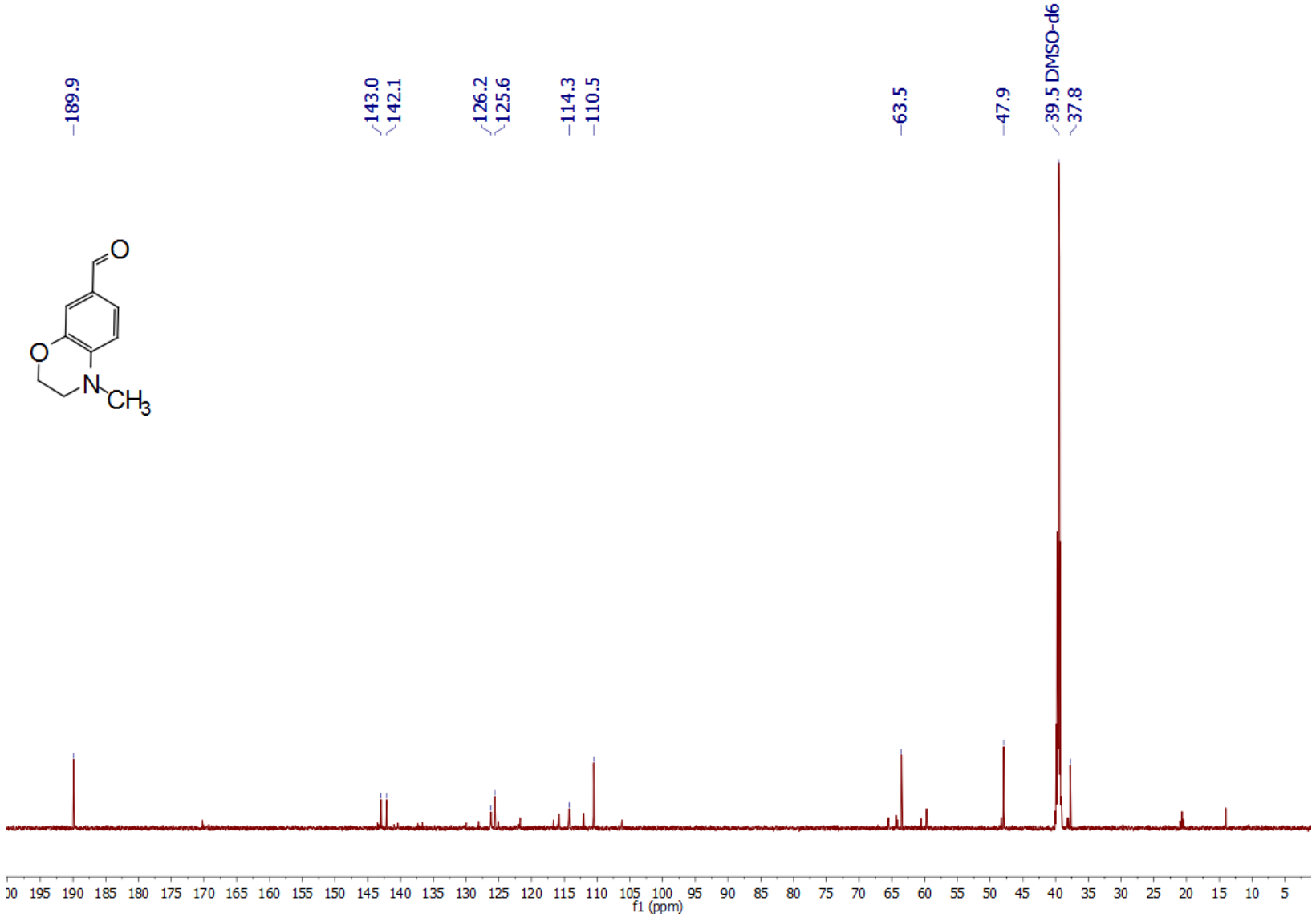

Supplementary S24. ^{13}C NMR spectrum of **SAI322** for synthesis of compound **3**.

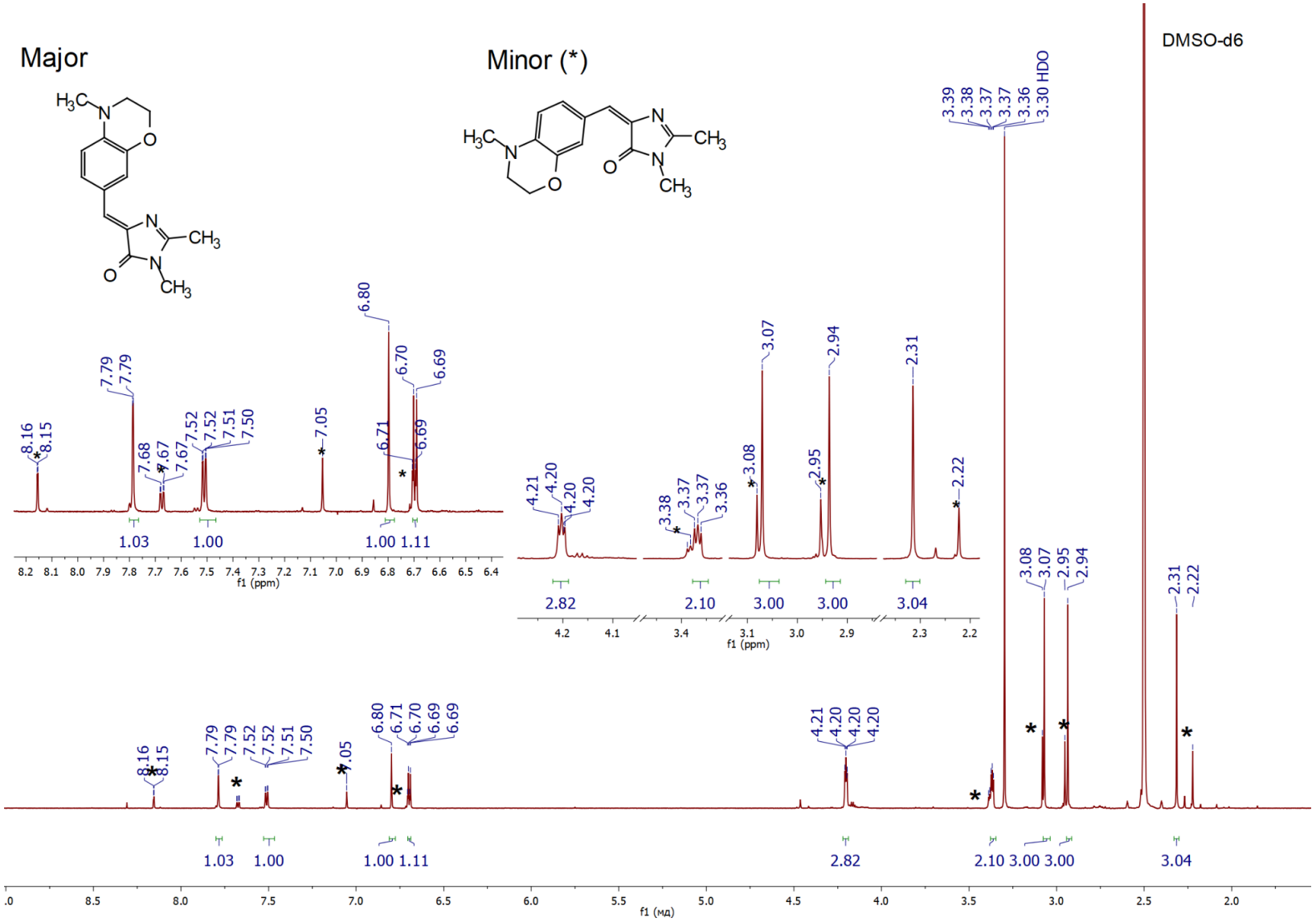

Supplementary S25. [1]H NMR spectrum of **SAI326** for synthesis of compound **3**.

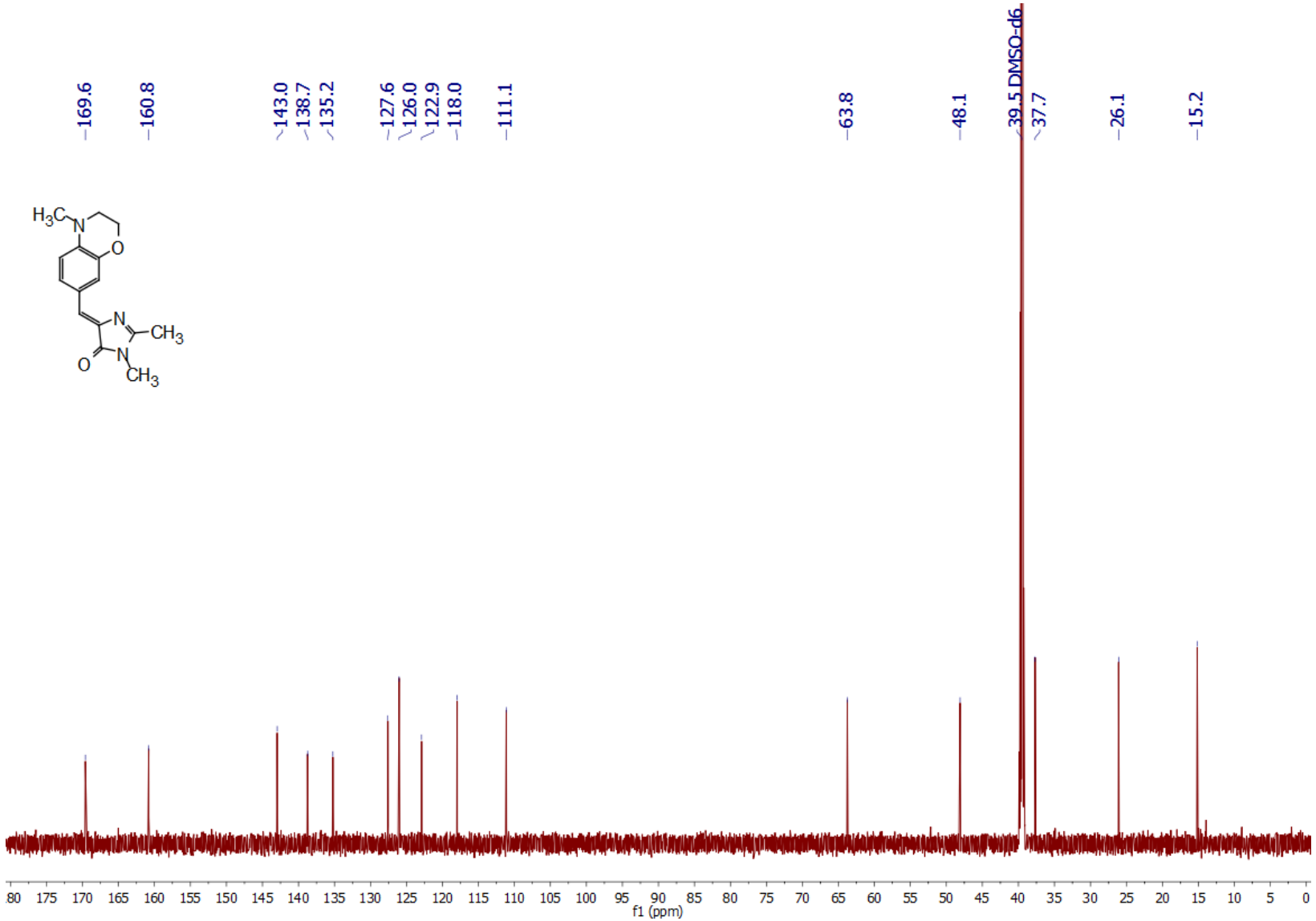

Supplementary S26. ^{13}C NMR spectrum of **SAI326** for synthesis of compound **3**.